Standing Wave Patterns in the CO Oxidation Reaction on a Pt(110) Surface: Experiments and Modeling†

Alexander von Oertzen,* Harm H. Rotermund, Alexander S. Mikhailov, and Gerhard Ertl

Fritz-Haber-Institut der Max-Planck-Gesellschaft, Faradayweg 4-6, D-14195 Berlin, Germany

Received: August 5, 1999; In Final Form: December 13, 1999

Standing waves are a special type of spatio-temporal pattern observed in the CO oxidation reaction on Pt(110). We present new experimental data that indicate the important role played by the formation of subsurface oxygen. The formation of these patterns is correlated with reflective collisions of traveling waves that have previously been found in the same reaction. We also show that global coupling through the gas phase and external forcing are essential for stabilizing and synchronizing the standing wave patterns. The principal properties of the observed patterns are reproduced by numerical simulations based on an extended reaction−diffusion model.

1. Introduction

The appearance of complex spatio-temporal patterns is a fascinating aspect of nonequilibrium chemical reactions. The classical examples of such patterns are traveling waves, target patterns, and rotating spiral waves in the Belousov−Zhabotinsky (BZ) reaction.[1−3] However, despite significant progress that has been made in understanding the BZ reaction, its detailed modeling remains difficult because of the complexity of its reaction scheme and the large number of intermediate products. In contrast to this reaction, the surface reaction of CO oxidation on Pt(110) is characterized by a simple mechanism and involves only a few reaction species.[4] This catalytic reaction is able to display the same basic patterns as the BZ reaction and, additionally, can show the new spatio-temporal pattern of *standing waves.*[5]

The standing waves represent an oscillatory pattern that consists of a periodic spatial array of bouncing concentration stripes.[5,6] Within one time period, every pair of adjacent stripes moves toward each other and merges together to form a single linear object that later splits and gives rise to two stripes that move in opposite directions. These two stripes collide, merge, and split again so that the initial pattern is repeated. A remarkable feature of the standing wave pattern is its perfect temporal synchronization over the entire crystal surface. This indicates that a mechanism that leads to rapid interactions between distant parts of the surface must be involved here. Already in the first publication about this phenomenon,[5] it was suggested that global coupling through the gas phase might play an important role in such spatio-temporal patterns. Experiments on the CO oxidation reaction with two separate Pd(110) samples demonstrated directly the operation of a synchronization mechanism by coupling through the gas phase.[7] It should be noted that, in experiments with electrically heated catalytic ribbons,[8−10] the gas-phase coupling has been identified as the important feature leading to pattern formation.

In contrast to reactions in aqueous solutions, such as the BZ reaction, the catalytic reaction of CO oxidation proceeds between adsorbed molecules on a solid surface. The structural properties of the Pt(110) single-crystal surface change during the course of reaction. Surface reconstruction, affected by the adsorption of CO, influences the adsorption rate for oxygen and, thus, provides a feedback loop that is responsible for the onset of oscillations and the excitable properties of this nonequilibrium reaction.[11] In addition, the reaction can induce facetting and roughening of the Pt(110) surface.[12,13] Another effect of the reaction is the formation of subsurface oxygen.[14−18]

We have recently shown[18] that, when subsurface oxygen is formed in relatively large amounts during the CO oxidation reaction on Pt(110), it not only significantly influences the quantitative properties of patterns, such as the propagation velocity of waves, but also leads to a number of new qualitative effects. Traveling waves show a special kind of collision behavior made possible only by the temporary storage of oxygen inside the metal and its subsequent release to the surface. This can explain the appearance of collisions that can be characterized as reflective (two-into-two) collisions of traveling waves or as the fusion of two colliding waves (two-into-one collisions).[18]

The CO oxidation reaction on Pt(110) has been described in the past by mathematical models that were gradually improved. Its principal general mechanism was elucidated about 20 years ago when molecular beam investigations[19] showed that this reaction proceeds via the Langmuir−Hinshelwood scheme, that is, both CO and oxygen must first adsorb before the reaction to produce CO_2 can take place. Results for the adsorption kinetics of oxygen[20−24] and those of CO[25−28] were reported at about the same time, when the first kinetic self-sustained oscillations on a single crystal were observed.[29] Understanding of the role of the phase transition[30−32] has finally led to the formulation of the first detailed model of this reaction.[33,34]

To reproduce the properties of the spatio-temporal pattern formation, this model has been extended to include diffusion of adsorbed CO molecules on the surface.[35,36] Simulations have shown that the model has solutions that correspond to traveling waves of chemical concentrations and that agree with the experimental observations.[36] It has also been found that most of this behavior can already be described[37] by a reduced version of the model that contains only two variables and represents a

† Part of the special issue "Gabor Somorjai Festschrift".

* Corresponding author. E-mail: oertzen@fhi-berlin.mpg.de. Fax: + 49-30-84 13 51 06.

10.1021/jp9927799 CCC: $19.00
Published on Web 03/15/2000

variant of the well-known FitzHugh−Nagumo model. This model has been successfully applied, for example, to understand properties of spiral waves under conditions of external forcing[38] and local modifications of the catalyst surface.[39,40]

Following the original suggestion[5] that standing waves are related to global coupling through the gas phase, Levine and Zou[41,42] modified the model by phenomenologically introducing gas-coupling terms. They proposed an explanation of standing waves as resulting from a parametric self-resonance caused by terms of the third order in the oscillation amplitudes. This special resonance is, however, found only under a very restrictive condition, specifically, in the vicinity of a certain codimension-two bifurcation, and is relatively weak.

Mikhailov et al. have shown that a standing wave pattern might naturally develop in oscillatory systems with global coupling for which the driving force is linear in the oscillation amplitude.[43,44] The effects that are observed in this case are much stronger and are not limited to the vicinity of a special codimension-two bifurcation point. These investigations have led to the prediction of new spatio-temporal patterns, such as cellular structures, that were also observed in the experiments with CO oxidation on Pt(110).[45] However, the investigations were performed in the framework of an abstract model based on the complex Ginzburg−Landau equation, and a detailed comparison with experimental data was, therefore, not possible.

Falcke and Engel have explicitly derived the gas-coupling terms in the kinetic equations[36] for the catalytic reaction under consideration.[46−48] They have also shown[46] how, in the vicinity of a supercritical Hopf bifurcation, this realistic model can be reduced to the complex Ginzburg−Landau equation with global coupling, such as that studied by Mikhailov et al.[43,44] The numerical simulations of the extended reaction−diffusion model of this reaction have shown a large variety of patterns, including spatio-temporal chaos and oscillations with phase domains. Nevertheless, the experimentally observed patterns of standing waves were not reproduced in these simulations, apparently indicating that some additional effects and mechanisms, not accounted for in their model, must be in operation when standing waves are formed.

In a parallel development, von Oertzen et al.[16] analyzed a different set of experiments, dealing with conversion of oxygen islands on Pt(110), and found that the experimental results can be reproduced only when the model is extended to describe the formation of a subsurface oxygen species. Importantly, the explanation of these experiments was only possible if it was assumed that conversion of oxygen into the subsurface species was strongly dependent on the structural state of the surface (taking place only on the non-reconstructed 1×1 surface) and that subsurface oxygen favored a lifting of the surface reconstruction. In a recent publication,[18] we have shown that, with the appropriate choice of parameters, the experiments with oxygen island conversion can be quantitatively reproduced using the suggested model modification.

If subsurface oxygen is formed under reactive conditions, this must have important consequences for the formation of non-equilibrium patterns. The principal effects are the delayed release of oxygen to the surface from the subsurface depot and the influence of subsurface oxygen on the surface structure that makes the surface more reactive. Indeed, our simulations for reactive conditions have allowed us to reproduce such observed processes as two-into-two and two-into-one collisions of traveling excitation waves.[18]

As soon as the reflective two-into-two collisions were found and theoretically explained, it became clear that the same effect might easily produce standing wave patterns. Indeed, if we start with a periodic array of colliding wave pairs, one might expect that, because of subsequent reflections, each wave would bounce between its neighbors and, thus, yield the behavior seen in the experiments. This idea had to be explored both experimentally and numerically.

With this aim, we have now conducted new, more detailed experiments that clearly show the emergence and the properties of standing waves. We have also performed experiments in which already existing standing waves were subject to external forcing that was produced by periodic modulation of the CO partial pressure. Our experiments reveal a close connection between standing waves and traveling excitation waves in the same system. Importantly, we were able to observe that standing waves can sometimes break down into a set of traveling wave fragments. The propagation velocities of traveling waves turn out to be close to the velocities of bouncing waves in a standing wave pattern. The parameter region in which standing waves are found is near the region in which reflective and merging collisions of traveling waves have been observed.

We observed that, whenever stable standing waves are found, their behavior on different parts of the surface is strictly synchronous within the observation window. We have seen that standing waves develop only on part of the surface, with the remaining surface area showing uniform oscillations with a rigidly correlated period and phase. Taking into account that the breakdown of the standing wave pattern was first accompanied by the disappearance of the synchronization, this result provides evidence that global coupling is necessary to stabilize a periodic array of bouncing waves.

After presenting, in the first part of this paper, the new experimental data, we proceed, in its second part, to describe the mathematical modeling of standing wave patterns using the extended reaction−diffusion model that includes the subsurface oxygen species and global coupling through the gas phase. The simulations reveal that, although standing waves may persist in an ideal system in the absence of global coupling, such patterns rapidly decay when surface defects are introduced. We show, however, that the patterns can be stabilized when external periodic forcing is applied. The forcing has been used to control the properties of standing waves, and the frequency entrainment effect has also been found. Furthermore, our simulations reveal that the role of external forcing can be played by periodic variations of the CO partial pressure because of kinetic reaction oscillations that take place on the surface outside the standing wave pattern.

The paper concludes with a comparison between the experimental data and the simulation results and a discussion of open questions and further research perspectives.

2. Experiments

2.1. Experimental Setup. The Pt(110) single-crystal sample had a disc shape with a diameter of 10 mm and, thus, had a surface area $A_s = 78.5$ mm^2. It was kept in an ultrahigh-vacuum (UHV) apparatus equipped with a low-energy electron diffraction (LEED) device, an Auger electron spectrometer, a differentially pumped quadrupole mass spectrometer, an Ar-ion sputtering gun, and resistive sample heating. The surface was prepared by Ar-ion sputtering and subsequent annealing to 1000 K. Successful preparation was verified by LEED and Auger spectroscopy. A photoemission electron microscope (PEEM)[49] provided information on the lateral distribution of adsorbed species on the surface.

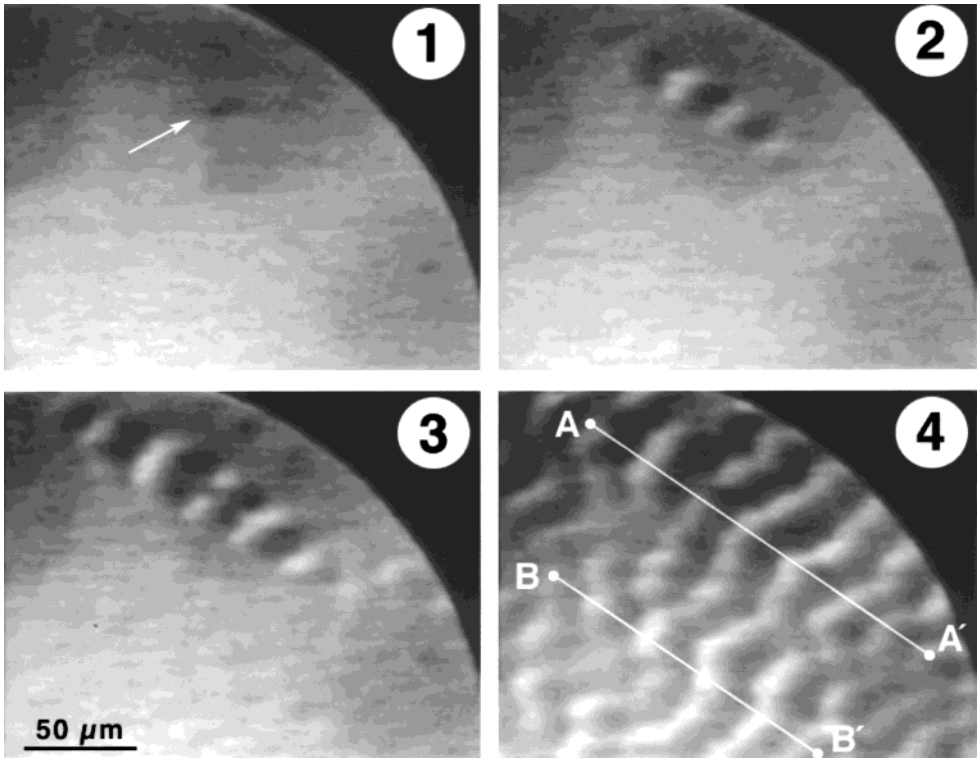

Figure 1. Development of standing waves from uniform oscillations. PEEM images of a surface area of size 212 μm × 166 μm are shown at times t = 0, 12.1, 15.4, and 22 s in frames 1−4, respectively. The reaction parameters are T = 528 K, $p_{CO} = 1.48 \times 10^{-4}$ mbar, and $p_{O_2} = 4.0 \times 10^{-4}$ mbar.

Gas supplies for CO and O_2, as well as pressure gauges, allowed for controlled dosing of the reactants into the UHV chamber (volume V_{Ch} = 60 L). Through a combination of feedback-regulated gas dosing and permanent pumping of the chamber, the catalytic reaction was made to proceed under constant-flow conditions. In front of the turbomolecular pump (pumping power j_p = 360 L/s) a valve was installed, which could be used to reduce the pumping power continuously. More details concerning the experimental and gas-dosing setup can be found in an earlier publication.[6]

The PEEM produces images of the distribution of photoelectron emission from a surface under ultraviolet light irradiation. With a maximum field-of-view of up to 500 μm in diameter, the spatial resolution of images is typically 1 μm. The PEEM is not directly sensitive to molecular adsorbate coverages, but instead images only the change of the work function of the clean surface due to the presence of an adsorbate. For the species under consideration, namely, adsorbed CO and O as well as subsurface oxygen, these work function changes are quantitatively known only for adsorbed CO and O. A full coverage by CO increases the work function of Pt(110) by 0.15 eV, thus reducing the photoemission signal. The presence of O_{ad} increases the work function by the larger value of 0.8 eV, yielding the lowest photoemission signal or, in other words, the darkest appearance in the PEEM images. For subsurface oxygen on Pt(110), an exact value of the work-function change has not been determined. This species, however, appears so bright in PEEM images that a pronounced work-function decrease can be concluded. In earlier work,[14] a decrease of about 1 eV for subsurface oxygen on Pt(100) was measured.

PEEM images can be viewed on the phosphorus screen of the image-intensifier unit by the bare eye. For later analysis, the entire temporal evolution of this image is recorded by a camera on S-VHS videotapes. Through the video system, the temporal resolution is limited to 40 ms. For the observed phenomena, this temporal resolution is sufficient. Standard image processing on single video frames, including background subtraction and contrast/brightness adjustments, was performed with a computer. Image averaging of two or four video frames could be applied in some cases to improve the signal-to-noise ratio in the images.

2.2. Observations of Standing Waves. In an earlier publication on pattern formation in the CO oxidation reaction,[5] only two frames of the standing wave pattern were included. The development of the stripe pattern from the uniform state was not analyzed at that time. Below, we present the detailed experimental data on the emergence and further development of standing waves.

Standing waves were recorded for sample temperatures between 520 and 550 K and with an O_2 partial pressure of 4×10^{-4} mbar and CO pressures of approximately 10^{-4} mbar. By sweeping the CO partial pressure, one can switch from the reactive and mainly oxygen-covered branch of the reaction to the CO-poisoned state with high CO coverage. In the mainly CO-covered regime, excitability for oxygen waves is found. In a narrow interval of CO partial pressures before a transition to excitable behavior, self-sustained uniform oscillations appear. Such oscillations were necessary precursors for standing waves, which then emerged within several minutes.

The development of standing waves is sensitive to variations in experimental conditions. Previous experiments with subsurface oxygen island conversions[18] seemed to enhance the probability of finding these patterns. Regions on a crystal where subsurface oxygen islands had been present earlier in the same experiment were preferred for the emergence of standing waves. A fine adjustment of the pumping rate via the main valve before the turbomolecular pump was sometimes needed to create standing waves.

Figure 1 shows four consecutive images of the development of standing waves at T = 528 K. In the first image, the surface

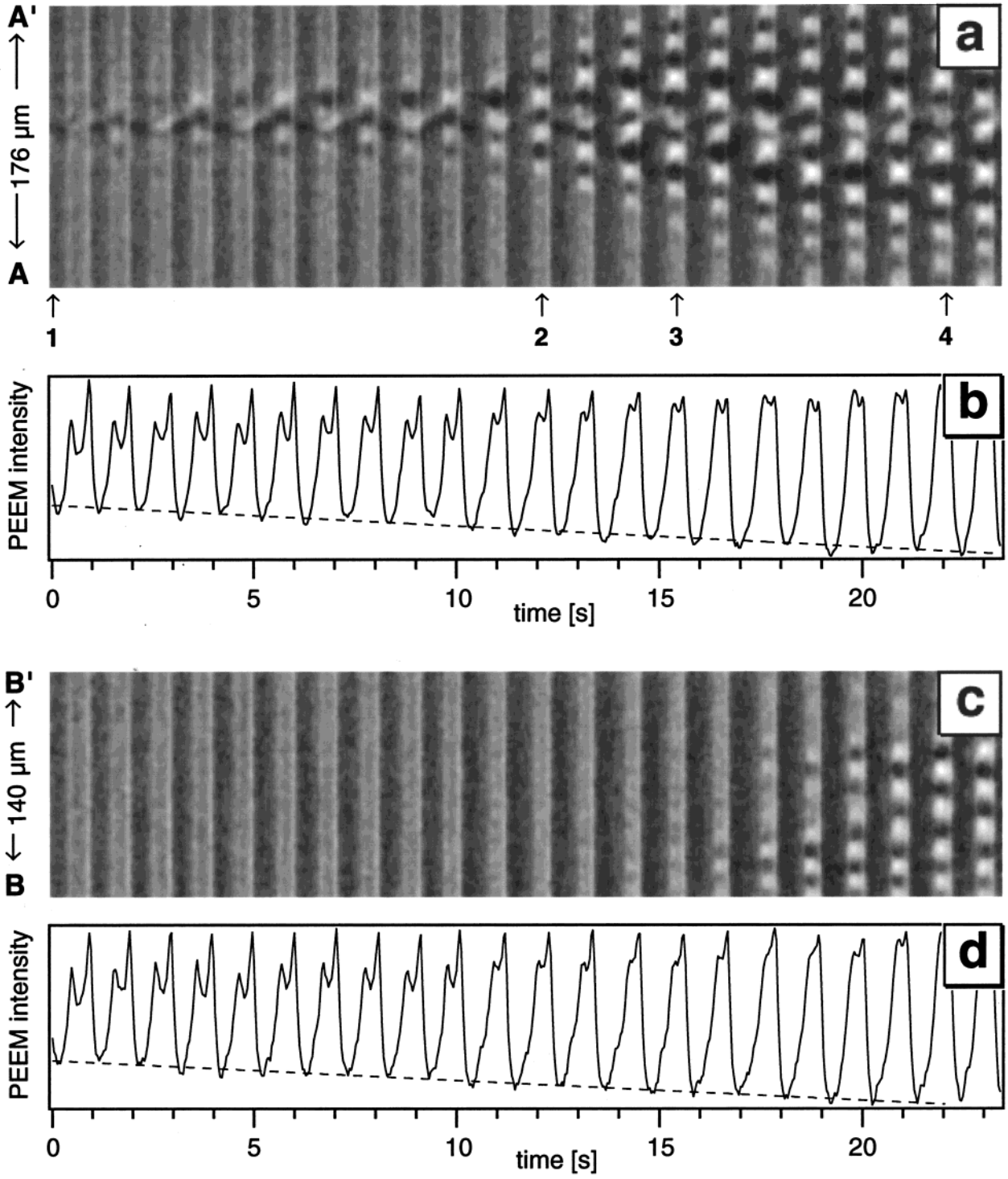

Figure 2. Temporal evolution of the PEEM intensity profile along lines (a) AA′ and (c) BB′ in Figure 1 and corresponding time dependences (b and d, respectively) of the average PEEM intensity along these lines. The time interval shown is 23.4 s; the lengths are (a) 176 μm and (c) 140 μm.

is found in a state of uniform oscillation. The white arrow points at a small surface defect. As can be seen in the second and third images, the properties of the region around the defect are slightly different, and a standing wave pattern starts to develop there. Meanwhile, uniform oscillations continue in the void area. Later, the standing waves spread and appear in the void region also. This state is shown in the last frame of Figure 1.

Panels a and c of Figure 2 show space−time diagrams corresponding to Figure 1. These space−time diagrams were constructed along lines AA′ and BB′ shown in the last frame of Figure 1. Intensity profiles along these lines were taken from consecutive video frames and assembled to form a space−time diagram. Time increases from left to right along the horizontal direction in this figure. Line AA′ passes through the defect, whereas line BB′ lies below it.

Synchronous uniform oscillations are clearly seen in the space−time diagrams of Figure 2. They persist while the pattern of standing waves emerges. Moreover, the processes in the region covered by standing waves are perfectly synchronized with the uniform oscillations taking place in the rest of the surface. Such strict synchronization, seen in sudden image intensity changes within less than one video frame (0.04 s), suggests that

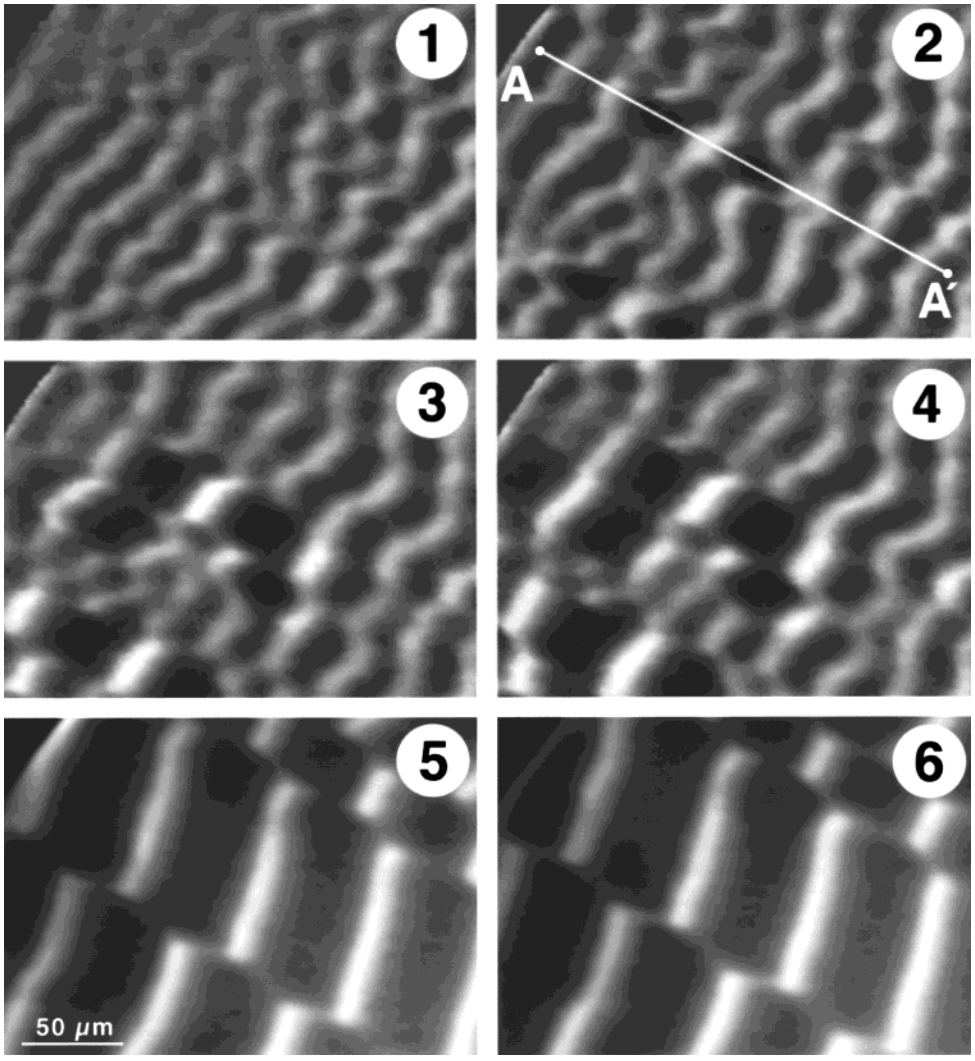

Figure 3. Doubling of the spatial period length in the standing wave pattern. PEEM images of a surface area of size 233 μm × 166 μm are shown at times $t = 0$, 12.8, 18.8, and 22.6 s in frames 1−4, respectively. Frames 5 and 6 were taken 3 min later and show the fully developed large-period standing wave pattern at two times separated by one-half period of oscillations. Same reaction parameters as in Figure 1.

a global synchronization mechanism exists. It can also be noticed that the pattern of standing waves slowly spreads across the surface, starting from the region where the defect is located.

Figure 2b,d displays the respective time dependences of the total PEEM intensity integrated along lines AA′ and BB′. We observe that kinetic oscillations were not constant in the experiment presented here. Instead, their profile gradually evolved from a double-peak shape toward a more simple, almost harmonical, type of oscillation. At the same time, the minimum level for each oscillation cycle (the dashed line) decreased at a constant rate, whereas the maximum level remained approximately constant.

In the experiment under consideration, the pattern of standing waves seen in Figure 1 represented only a transient stage and, through a secondary instability, was replaced by a different standing wave pattern with a doubled spatial period. This secondary instability and the development of the new pattern are illustrated in Figure 3. The first frame in this figure was taken a few seconds after the last frame in Figure 1. Note that images are now taken from a different section of the imaged area.

The first four images in Figure 3 are separated by short time intervals and show how a standing wave pattern with a larger spatial periodicity originates locally and begins to spread. The last two images were recorded 2 min later. They display a fully developed large-period pattern (such images were presented as examples of standing waves in the initial publication[5]). The spatial period of the standing waves was 24 μm before the transition and 53 μm after the transition. Hence, it was actually slightly larger than the doubled period (48 μm). The temporal period of the standing waves did not change after the transition and remained close to 1 s.

The considered transition is clearly seen in the space−time diagram in Figure 4. It has been constructed in the same way as the diagrams in Figure 2 along line AA′ in the second frame in Figure 3. We note that the area occupied by double-periodicity waves gradually spreads on the background of the initial pattern. This process continues until the entire pattern is transformed. When the sample was moved in front of the PEEM, it became evident that, after the transition, only standing waves with the larger spatial period were present on the surface. However, some parts of the surface remained in the uniformly oscillating state even in this case.

Oscillations with the large-period standing wave pattern were followed in the experiment for about 1 h. The standing waves were highly regular. The pattern in Figure 5 shows two single frames of the standing wave pattern and the corresponding space−time diagram in this final regime.

Another interesting behavior of standing waves was observed in an experiment performed at a slightly different temperature, $T = 523$ K, and at a lower CO partial pressure. Figure 6 shows

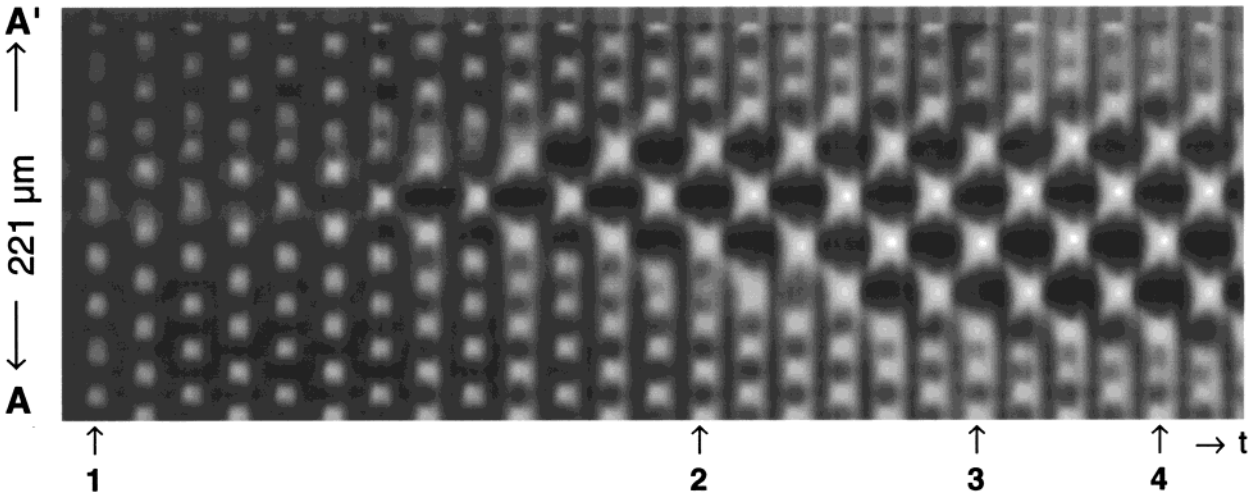

Figure 4. Temporal evolution of the PEEM intensity profile along line AA′ in Figure 3. The time interval shown is 25.2 s; the length of line AA′ is 221 μm.

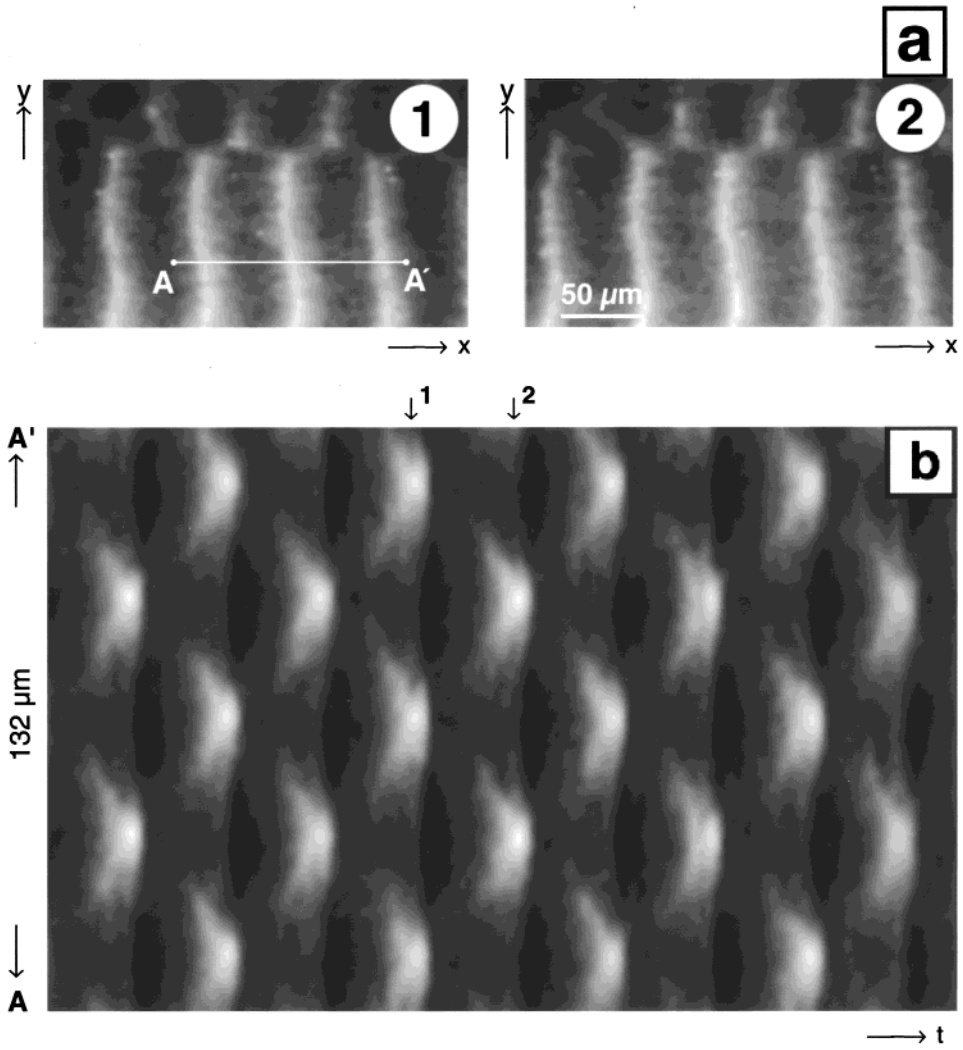

Figure 5. (a) Two snapshots of an established standing wave pattern. PEEM images of a surface area of size 254 μm × 148 μm, separated by time interval $\Delta t = 1.1$ s. (b) Corresponding space−time diagram constructed along line AA′. The time interval shown is 10 s; the length of line AA′ is 132 μm. The temporal positions of the two frames in (a) are indicated by arrows in (b). Same reaction parameters as in Figure 1.

the space−time diagram for a representative linear cross section perpendicular to the standing wave pattern. The total recorded time was 800 s, so that each of the five subsequent segments corresponds to time intervals of 160 s.

In this experiment, we found the pattern in the presence of oscillations while searching the surface by moving the sample in front of the microscope. Thus, the initial process leading to the formation of standing waves has not been recorded. As we

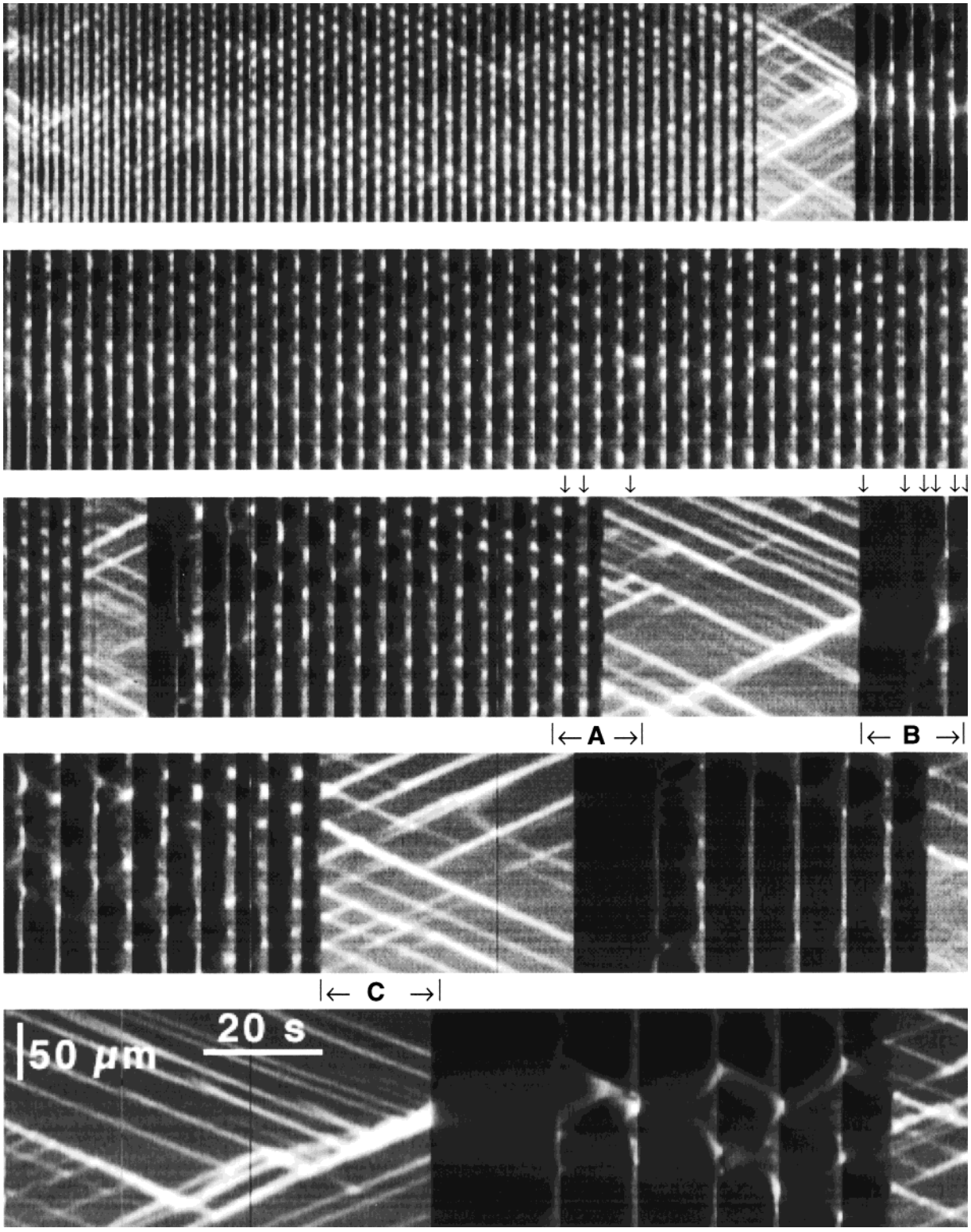

Figure 6. Space−time diagram for a long sequence of PEEM video frames. The reaction parameters are $T = 523$ K, $p_{CO} = 1.29 \times 10^{-4}$ mbar, and $p_{O_2} = 4.0 \times 10^{-4}$ mbar. The total time interval is 800 s; the spatial extension is 194 μm. For convenience, the diagram is split into five segments that are placed one under another, with later times corresponding to lower-lying segments.

see in the top segment in Figure 6, the oscillating pattern persists for some time. Its temporal period slowly increases, and then suddenly, the global oscillations disappear. At this point, standing waves immediately break down and transform into a system of *traveling waves* (we discuss this instability below).

The oscillations could be re-established by a slight decrease in the CO partial pressure. The moment at which this occurred can be identified by the sudden change of the image intensity to the darker level in the upper segment in Figure 6. The new oscillations have a larger temporal period. They lead to the re-emergence of standing waves, which occupy the entire second segment in Figure 6. Later, the oscillations stop (the left part of the third segment), and the standing waves again disappear. After a while, the CO partial pressure was again increased, leading to the repetition of the cycle described above. Altogether, Figure 6 shows six intervals of standing waves, each ending

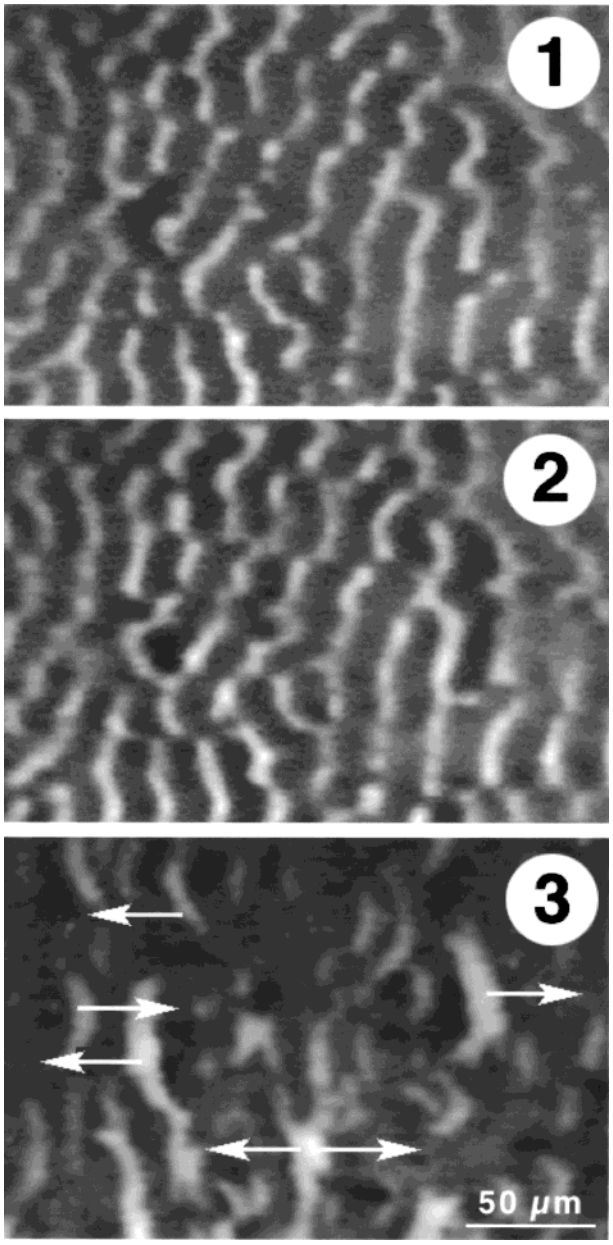

Figure 7. Breakup of the standing wave pattern. Single PEEM images of a surface area of size 236 μm × 150 μm are taken at three consecutive times, as indicated by small black arrows in the time interval marked by the letter A in Figure 6. White arrows in frame 3 indicate the direction of motion of traveling wave fragments produced after disintegration of the standing wave pattern.

with the disappearance of oscillations and the disintegration of the standing wave patterns.

To illustrate the breakup of standing waves, we display in Figure 7 three subsequent images taken from the interval marked by the letter A in the space−time diagram in Figure 6. The first frame shows a pattern of standing waves. These waves start to develop a transverse modulation (frame 2) and suddenly break into a set of propagating wave fragments that move in both directions and are indicated by arrows in frame 3. This process can also be viewed as a computer video at the Internet page http://www.fhi-berlin.mpg.de/~complsys. (See also Supporting Information.)

The propagating wave fragments correspond to straight, bright lines in the space−time diagram in Figure 6. The slopes of these lines are equal within experimental error, implying that all such fragments move at practically the same velocity. Moreover, the moving fragments do not annihilate under frontal collisions. Instead, they "pass" through one another and sometimes also merge. This soliton-like behavior strongly resembles the corresponding properties of bright traveling waves, which were investigated in our previous paper[18] and attributed to the formation of subsurface oxygen. Such waves, bearing large amounts of subsurface oxygen, can indeed display two-into-one collisions, in which the two objects merge to form a single wave. They can also show two-into-two collisions, which were called reflections in the earlier paper. The soliton-like behavior in the CO oxidation reaction that was reported earlier[50] involved a different type of oxygen wave, which appears black in the PEEM image. The penetration of two dark oxygen waves was a quite rare event and could only be explained by simulations when a special defect at the location of the collision was assumed.[35]

The re-emergence of a standing wave pattern after a decrease of the CO partial pressure in the experiment described above is illustrated in the series of images in Figure 8, which correspond to the interval marked by the letter B in the space−time diagram of Figure 6. The first frame shows the surface predominantly covered by oxygen. In frames 2−4, the growth of irregularly shaped islands can be seen. These islands are formed inside the oxygen-covered area and, therefore, contain CO. As the growing islands come into contact, bright structures develop along the contact lines (frames 5 and 6). Subsequently, these bright structures become ordered into a set of stripes and give rise to a standing wave pattern.

It is remarkable that this process is quite similar to one that was described in our previous publication.[18] In that case, the bright structures, formed at the contact lines of colliding oxygen islands, gave rise to traveling wave fragments (cf. Figure 4 in ref 18). It seems, therefore, obvious to suggest that the difference in the observed behavior, which, in the present experiment, consisted in the transformation of such bright structures into a system of standing waves, is related to the presence of periodic kinetic oscillations. These oscillations bring about the pattern of standing waves. When they disappear, the pattern immediately degenerates into a system of propagating waves, as seen in Figure 7.

As a consequence of this conclusion, the standing wave phenomenon can be rationalized as a pattern that is formed by periodically colliding and reflecting subsurface oxygen waves and that is maintained and synchronized through kinetic oscillations. Moreover, the individual properties of such bouncing waves should, therefore, not be much different from those of single traveling-wave fragments.

To test this suggestion, we have compared the propagation velocity of traveling waves, observed in the absence of oscillations, with the effective velocity of bouncing pulses in the standing wave patterns. The velocity of traveling waves was evaluated as the slope of the straight lines in Figure 6 during the time intervals when kinetic oscillations were absent. The effective velocity of bouncing pulses was calculated as the ratio of the spatial and temporal period of standing waves (assuming that a pulse passes a distance equal to the spatial period of the pattern within a single temporal period). These effective velocities were computed for each of the intervals in Figure 6 in which kinetic oscillations were present.

The results are shown in Figure 9 for the entire observation time of 800 s. The open circles indicate the velocities of traveling waves, and the filled circles show the effective velocities of bouncing pulses in standing wave patterns. We see that both velocities are equal within the measurement precision, marked

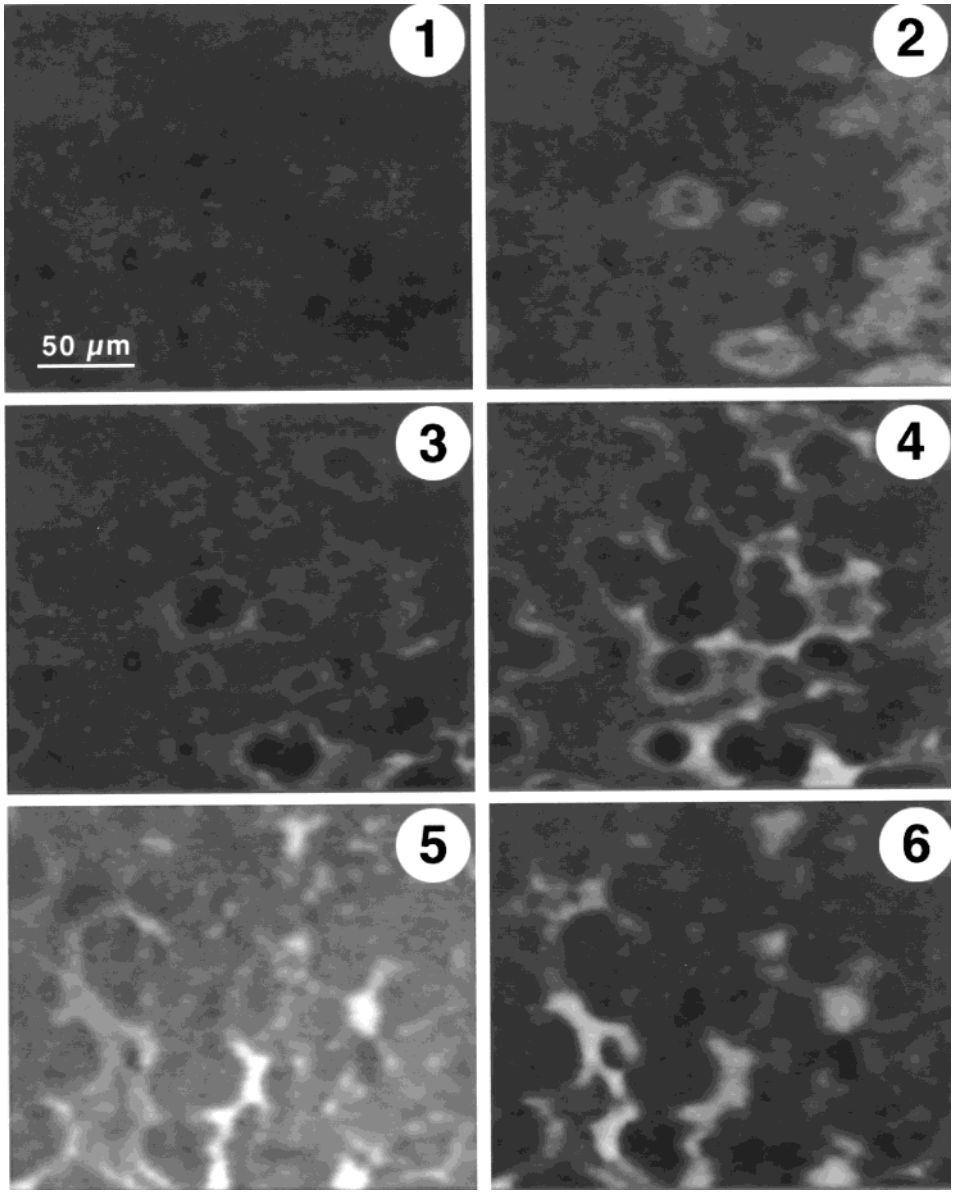

Figure 8. Re-emergence of standing waves after an adjustment of the CO partial pressure. Single PEEM images of a surface area of size 236 μm $\times$ 150 μm are taken at six consecutive times, as indicated by small black arrows in the time interval marked by the letter B in Figure 6.

by vertical bars in this figure. A slow trend toward smaller propagation velocities reflects the drift of experimental parameters.

This result supports the conclusion that subsurface oxygen plays an important role in the standing wave pattern. We note a certain similarity between such patterns and propagating waves of subsurface oxygen. This conclusion will be confirmed by numerical modeling of standing waves in the second part of this paper.

At the end of this section, we present additional examples of standing waves that were observed in experiments at different temperatures. Figure 10 shows standing waves recorded at a relatively low temperature, $T = 508$ K. A typical image (left side) and the corresponding space−time diagram (right side) constructed along the central vertical line in this image are displayed. We see that standing waves occupy only part of the image area and that uniform oscillations are taking place in the rest of it. The oscillation period is 5.0 s. Examining the temporal variation of intensity levels in the uniformly oscillating lower part of the image, we notice that these kinetic oscillations are not harmonic, but rather are of a relaxational type. Further on, this space−time diagram clearly shows repeated splittings and collisions of waves. Such splitting and subsequent joining occur during those intervals of the oscillation period when the surface is found in the darker state.

Standing waves have been observed up to the temperature of $T = 564$ K. The standing waves at this highest temperature are displayed in the space−time diagram in Figure 11. The oscillation period in this case is 1.1 s.

2.3. Standing Waves under External Forcing. External forcing of the CO oxidation reaction was investigated shortly after self-sustained oscillations had been discovered in this reaction.[51,52] In those investigations, the oxygen partial pressure was modulated with a harmonic signal of varying period and amplitude. The reaction state of the surface was monitored with a Kelvin probe, yielding information on the work function averaged over the entire surface. The response of the reaction to external forcing was interpreted in these studies within the framework of the general theory of frequency locking and resonant entrainment in oscillatory systems. The spatially resolved images of the reacting surface could not be obtained in such

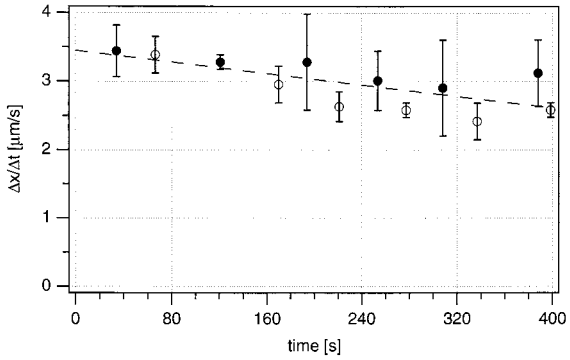

Figure 9. Velocity of traveling waves (open circles) and effective velocity of bouncing pulses in the standing wave pattern (filled circles) determined by analysis of the space−time diagram of Figure 6. Vertical bars show experimental errors.

early experiments, and therefore, one cannot definitely say what types of spatio-temporal patterns were subject to external forcing. However, it seems highly probable that these experiments dealt only with uniform kinetic oscillations. Indeed, standing waves are found only within a narrow parameter interval.

We report, in this section, the results of our new experiments, in which the influence of external forcing on standing waves has been investigated. The PEEM was used, in this case, to identify the situations in which standing waves persisted or became destroyed. Forcing was provided by periodic modulation of the CO partial pressure in the reaction chamber. The CO partial pressure at the gas inlet was recorded by using a voltage-frequency converter and storing the signal in parallel on the audio track of the videotape that was used to store the temporal evolution of the PEEM images. The absolute range of CO partial-pressure variation was recorded on the other audio track by oral comments. In a typical experiment, the CO partial pressure periodically varied around the 1.7×10^{-4} mbar level with an amplitude of 1.8%. Standing waves were allowed to develop before forcing was applied. Thus, the frequency of the autonomous oscillations was known beforehand, and this information was used to choose the appropriate forcing frequency.

Application of external forcing with the frequency of autonomous oscillations resulted in locking their phases to the external signal. This is seen in Figure 12, where external forcing of the CO partial pressure with a frequency of 0.8 s^{-1} is applied. The CO partial pressure at the gas inlet is displayed as a graph below this space−time diagram. The corresponding space−time diagram of standing waves in the absence of external forcing, but otherwise under the same experimental conditions, is shown in Figure 11. We have found that the maximum in the curve of external CO partial pressure coincides with the stage at which collisions of bright pulses are observed.

In an additional experiment, we reduced the forcing frequency in small steps, beginning with the frequency of the autonomous oscillations. The frequency locking of the standing waves to the external periodic signal was observed in this case down to the modulation frequency of 0.4 s^{-1}. Figure 13 shows an example of a space−time diagram for the modulation frequency of 0.5 s^{-1} (the frequency of autonomous oscillations is 0.9 s^{-1}). Sometimes, phase jumps occurred when the difference between the natural and the external frequency was as large as in this case. Such a phase jump can be seen in Figure 13 at the beginning of the space−time diagram.

Thus, external periodic forcing is very effective in controlling the properties of a standing wave pattern. However, the

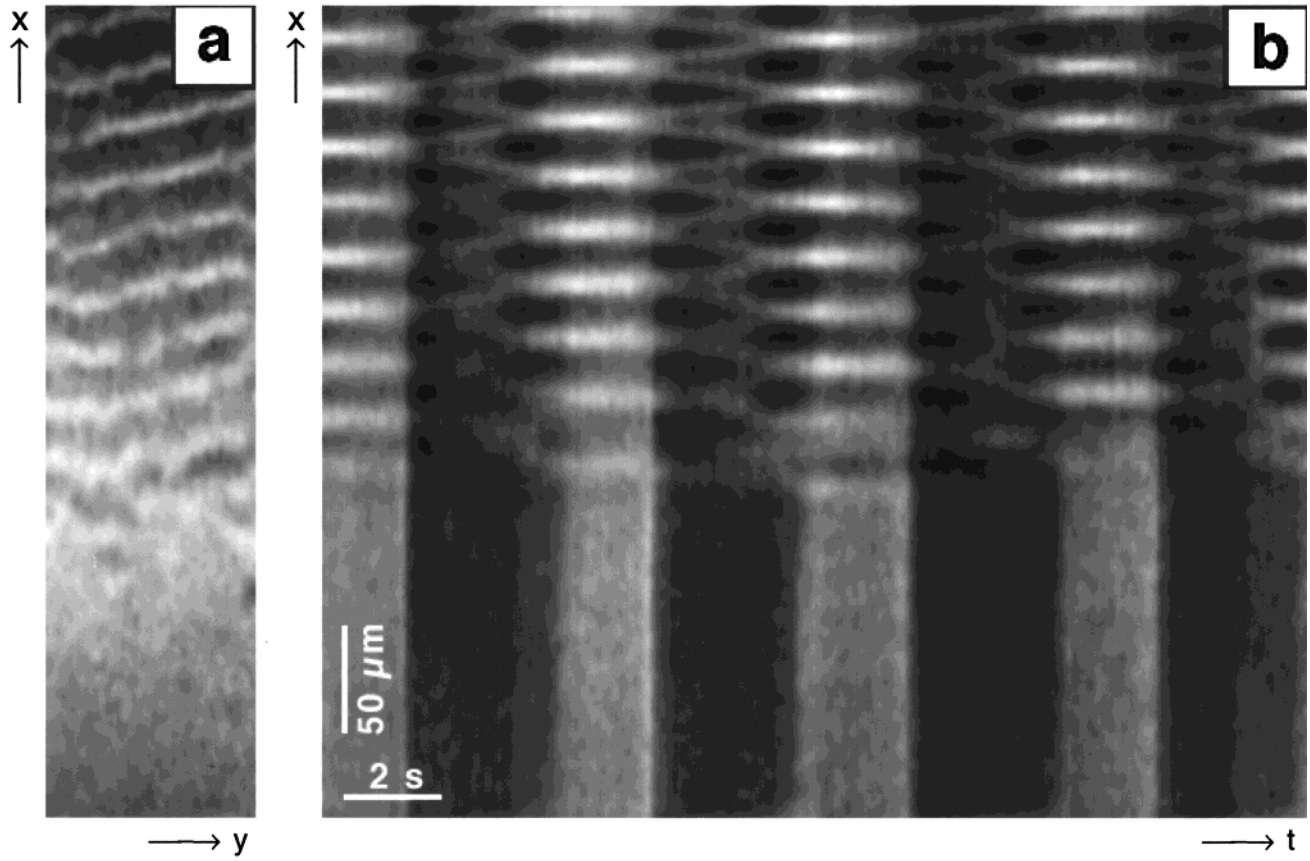

Figure 10. (a) PEEM image of a standing wave pattern in an area of size 95 μm × 370 μm. (b) Corresponding space−time diagram of the PEEM intensity profile along the central vertical cross section in this image during a time interval of 20 s. The reaction parameters are $T = 508$ K, $p_{CO} = 8.7 \times 10^{-5}$ mbar, and $p_{O_2} = 2.0 \times 10^{-4}$ mbar.

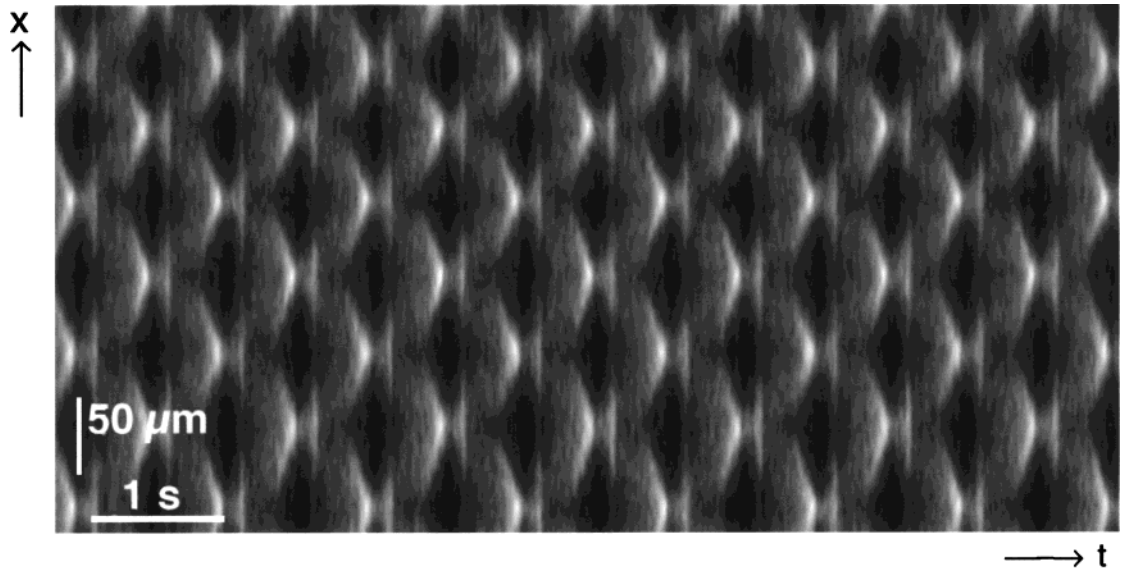

Figure 11. Space−time diagram of standing waves. The reaction parameters are $T = 564$ K, $p_{CO} = 1.7 \times 10^{-4}$ mbar, and $p_{O_2} = 4.13 \times 10^{-4}$ mbar. The time interval shown is 16 s; the cross-section length is 346 μm.

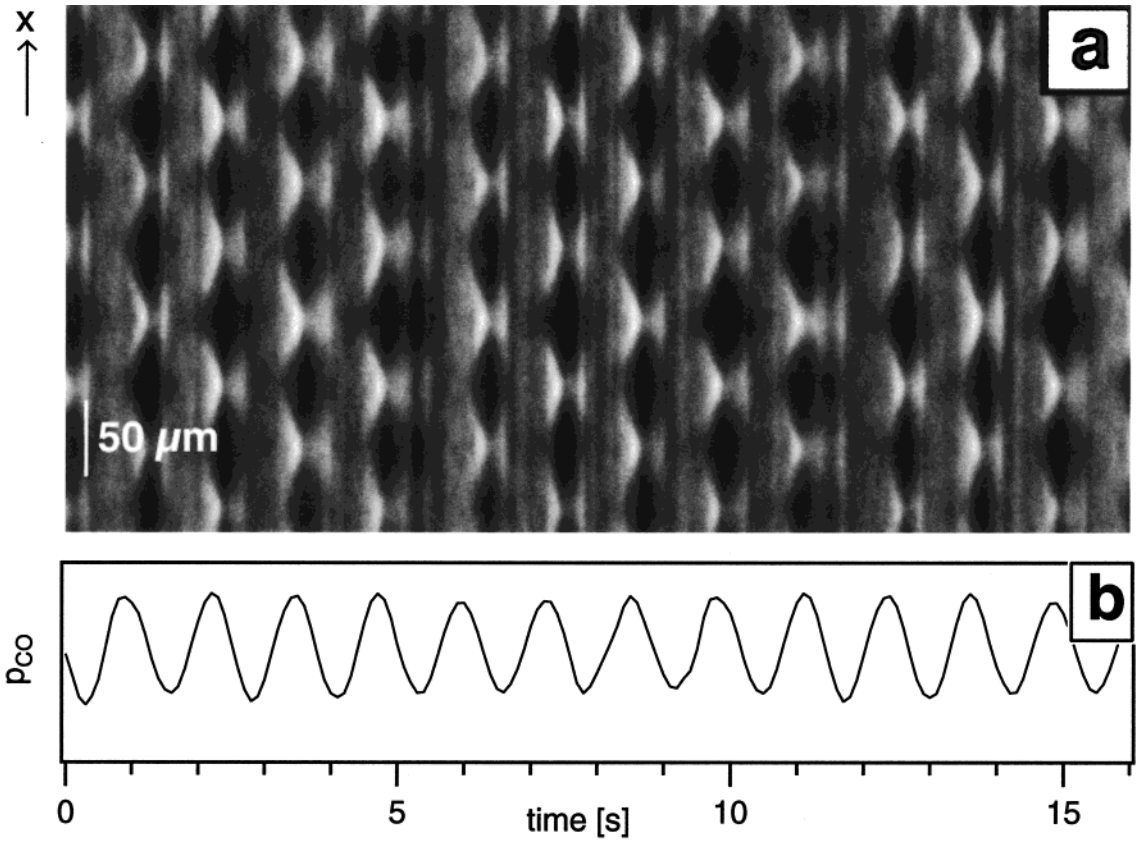

Figure 12. (a) Space−time diagram of standing waves under external forcing. (b) Corresponding periodic modulation of the CO partial pressure. The reaction parameters are $T = 564$ K, $p_{CO} = 1.7 \times 10^{-4}$ mbar, and $p_{O_2} = 4.13 \times 10^{-4}$ mbar. The frequency of external forcing is $f = 0.8$ Hz. The time interval shown is 16 s; the cross-section length is 346 μm.

amplitudes of forcing needed to produce the synchronization are low and are comparable to the estimated magnitude of variations of the CO partial pressure in the reaction chamber for kinetic oscillations of the surface reaction under consideration. When describing experimental observations of standing waves in the previous section, we saw that only part of the surface was usually covered by this pattern, while the rest of the area was in the state of uniform oscillations. This leads us to question whether uniform oscillations on other parts of the surface provide external forcing that acts on the standing waves and stabilizes this pattern.

To a certain extent, this question was already answered positively in the previous section, when we noticed that the standing wave pattern is always perfectly synchronized with uniform oscillations and immediately breaks down when the oscillations disappear. Now, we want to further investigate this

aspect of the problem and to analyze the precise phase relation between the variations of CO partial pressure in autonomous kinetic oscillations and the standing wave pattern influenced by them.

For this purpose, quantitative information on the magnitude and phase of partial-pressure variations should be collected. We have, therefore, continuously measured the CO partial pressure with a quadrupole mass spectrometer (QMS) during oscillations. The high partial pressure of oxygen, however, allowed us to use the QMS only for relatively short periods of time, because the prolonged usage of this device would have yielded rapid destruction of the emission filament. Hence, full exploration of the parameter space has not yet been undertaken.

Figure 14a shows a space−time diagram of a pattern that occupies part of the surface and is surrounded by the area with uniform oscillations. Although the pattern is irregular, we can still roughly classify it as a pattern of standing waves. Indeed, bright colliding and reflecting pulses are seen in the diagram, and their motion is correlated with the uniform oscillations.

When this pattern was observed, the QMS was switched to mass 44 for CO_2, and the QMS signal was recorded via a frequency signal on the audio track. This frequency signal was back-converted and plotted directly below the space−time diagram in Figure 14b. It varies by ±2.4% around $p_{CO_2} = 2.1 \times 10^{-8}$ mbar. The phase relation can be deduced from the figure and is such that the phase of lowest CO_2 production coincides with the sharper pattern.

After this recording, the QMS was switched to mass 28 for CO, and the QMS signal was again recorded. The second part of the plot in Figure 14b shows this CO signal. The amplitude is only 0.27%, and hence, the signal is distorted by more noise. Obviously, however, such a small variation of the partial pressure of one of the reactants caused by the oscillatory kinetics already suffices to synchronize the entire surface by global coupling. The dotted line was drawn to indicate the periodic behavior. Here, the relation between the CO signal and the pattern is such that a high value of the CO partial pressure coincides with the sharp appearance of the pattern.

The observations made for the phase relations of both partial pressures are in agreement. When the CO_2 partial pressure drops, the overall reactivity must be smaller, and at the same time, the CO partial pressure must rise, as less CO is consumed.

3. Modeling of Standing Wave Patterns

3.1. The Kinetic Model. The model for the CO oxidation reaction on Pt(110) is based on a decomposition of the entire reaction into elementary steps. These steps include the adsorption, desorption, and diffusion of CO; the adsorption of oxygen; the surface reaction; the structural phase transition; and the formation of subsurface oxygen. Independent studies of each of these processes have been previously conducted, yielding detailed data about their characteristic rates. In the original model by Krischer and Eiswirth,[33,34,53] the surface coverages of CO and O and the fraction of surface reconstruction represent the basic variables. Their temporal evolution is described by a set of differential equations, deduced from the experimental data.

We have recently extended this model to account for the observation of subsurface oxygen formation in island-conversion experiments[16] and to account for traveling subsurface oxygen waves.[18] This model includes the concentration of subsurface oxygen as a new variable. Formation of subsurface oxygen from the surface oxygen species and its back transformation are additional processes that are taken into account.

According to our previous analysis,[16,18] the formation of subsurface oxygen takes place only on the non-reconstructed 1 × 1 surface. Hence, its rate is proportional to the local fraction of non-reconstructed area. Moreover, it is assumed in the model that oxygen atoms can occupy only a single subsurface level that lies directly under the surface. Therefore, the conversion rate is also proportional to the number of free sites in this layer. We have found that the rate of back transformation is independent of the local CO coverage and depends only on the number of surface sites not covered by oxygen. Hence, in contrast to adsorption of oxygen from the gas phase, the CO molecules sitting on the surface do not prevent the return of oxygen to the surface from the subsurface level.

An essential aspect of the extended model[16,18] is that subsurface oxygen influences the structure of the surface. Similar to adsorbed CO molecules, subsurface oxygen favors the lifting of the surface reconstruction, that is, the formation of the 1 × 1 phase. Similar to the effect due to CO coverage in the original model, this influence of subsurface oxygen becomes significant only at sufficiently high concentrations of subsurface oxygen.

Under certain experimental conditions, specifically when the pumping rate is reduced, feedback via the CO partial pressure can become significant. The UHV chamber is used as a flow reactor with constant rates of supply and removal of the educts under equilibrium conditions. If, however, the removal of the educts by the reaction reaches a sufficient magnitude and also varies with time, these effects must be included in the model. Then p_{CO}, which previously was a control parameter, will be one of the variables of the model accounting for global feedback.

The following equations constitute the kinetic model used in our numerical simulations. Here, the variable u denotes the local CO coverage, v represents the surface oxygen coverage, and s represents the local concentration of subsurface oxygen; all three of these properties can vary in the interval from 0 to 1. The variable w describes the local structural state of the surface. Its extreme values, $w = 0$ and $w = 1$, correspond to the reconstructed 1 × 2 and non-reconstructed 1 × 1 phases, respectively. The intermediate values of w correspond to microscopic mixtures of both phases. Hence, this variable generally specifies the local fraction of the surface area found in the non-reconstructed phase. The equations are the following:

$$\frac{\partial u}{\partial t} = k_1 s_{CO} p_{CO}(1 - u^3) - k_2 u - k_3 u v + D_x \frac{\partial^2 u}{\partial x^2} + D_y \frac{\partial^2 u}{\partial y^2} \quad (1)$$

$$\frac{\partial v}{\partial t} = k_4 p_{O_2}[s_{O,1\times1} w + s_{O,1\times2}(1 - w)](1 - u - v)^2 - k_3 u v - k_6 v w(1 - s) + k_7 s(1 - v) \quad (2)$$

$$\frac{\partial w}{\partial t} = k_5[f(u,s) - w] \quad (3)$$

$$\frac{\partial s}{\partial t} = k_6 v w(1 - s) - k_7 s(1 - v) \quad (4)$$

$$\frac{\partial p_{CO}}{\partial t} = \gamma(p_{CO}^0 - p_{CO}) - \chi \int_{A_{mod}} [k_1 s_{CO} p_{CO}(1 - u^3) - k_2 u]\, da \quad (5)$$

These equations contain various terms corresponding to different processes that affect the concentrations of reacting species and influence the state of the surface. The processes taken into account in eq 1 are adsorption of CO, desorption of CO, reaction of CO_{ad} with O_{ad}, and diffusion of adsorbed CO molecules on the surface. Equation 2 includes the terms corresponding to adsorption of oxygen, reaction of O_{ad} with CO_{ad}, formation of subsurface oxygen, and back conversion. Equation 3 describes the dynamics of the phase transition

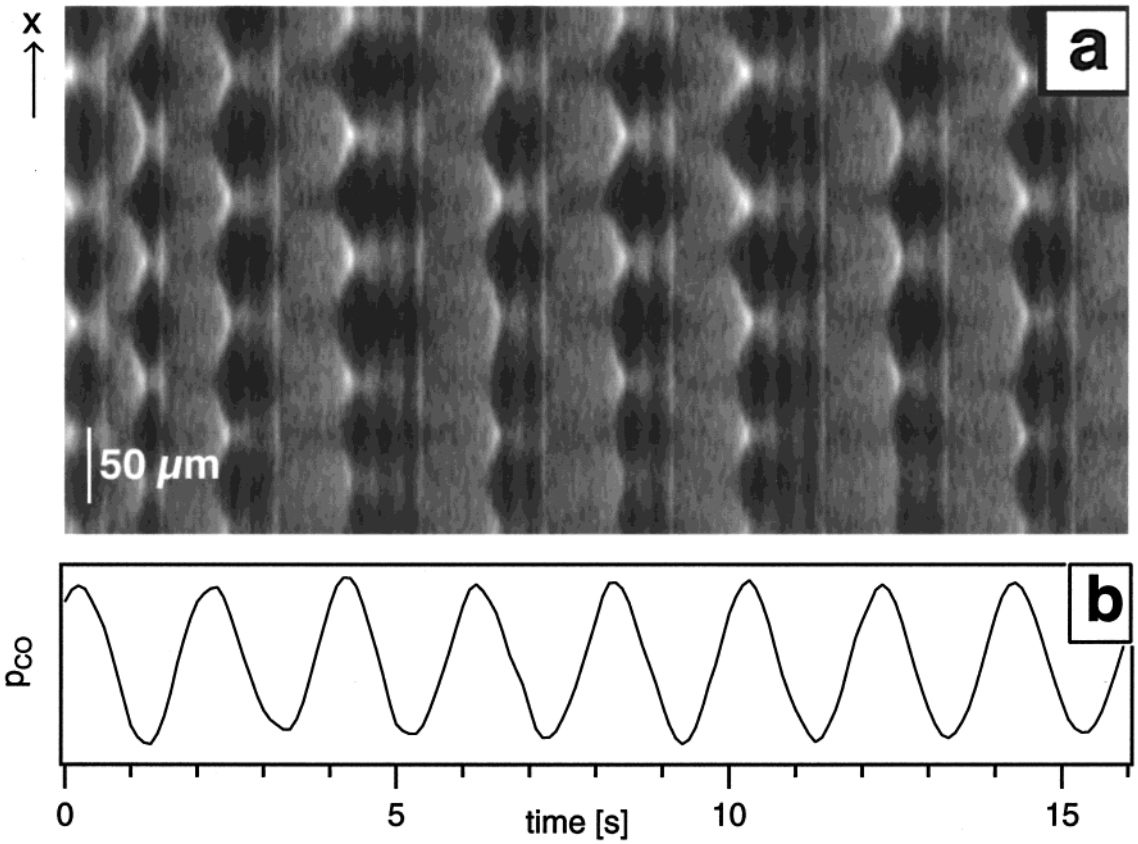

Figure 13. (a) Space−time diagram of standing waves under external forcing. (b) Corresponding temporal modulation of the CO partial pressure. Same reaction parameters as in Figure 12, but the frequency of external forcing is $f = 0.5$ Hz. The time interval shown is 16 s; the cross-section length is 346 μm.

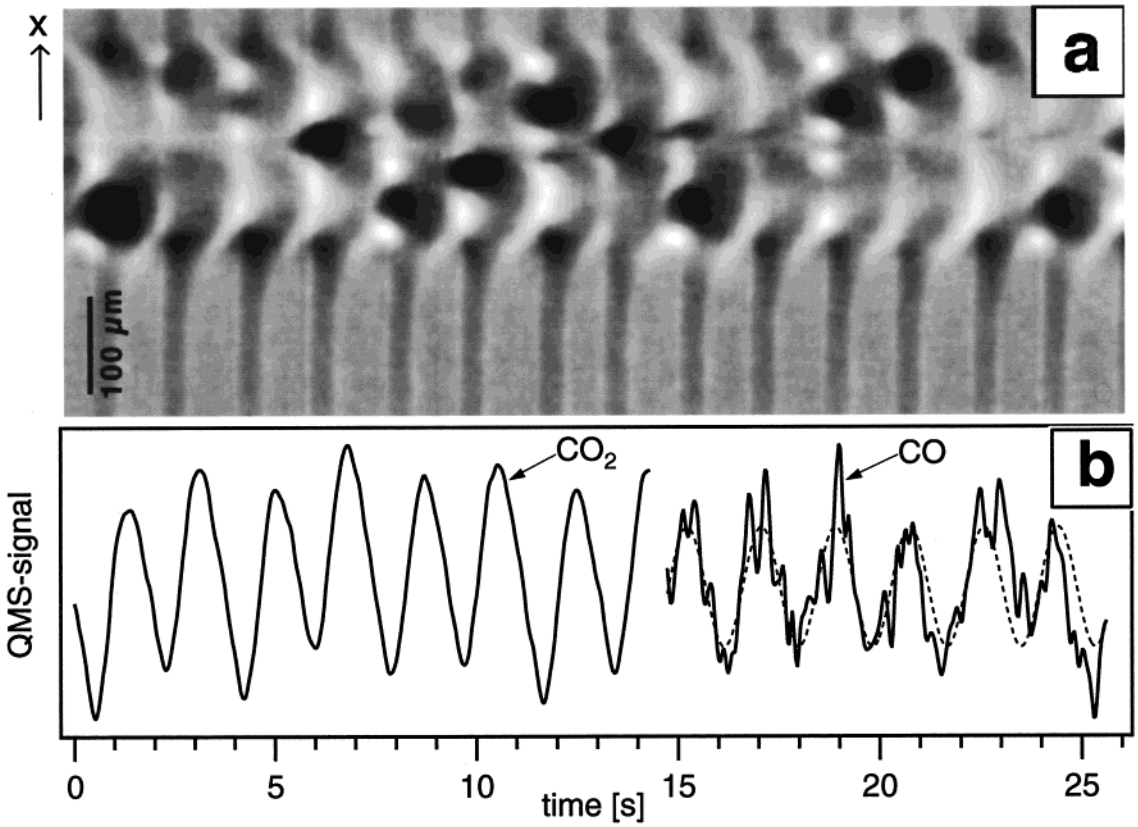

Figure 14. Intrinsic forcing of standing waves. (a) Space−time diagram of duration 26.6 s through a cross section of length 250 μm showing standing waves and uniform oscillations. (b) Plots of the measured temporal variation of CO_2 production (left) and CO partial pressure (right) in arbitrary units. The relative variations are $\pm 2\%$ for CO_2 and $\pm 0.15\%$ for CO. The dotted curve shows a sine-function fit for the CO partial pressure variation. The reaction parameters are $T = 546$ K, $p_{CO} = 1.8 \times 10^{-4}$ mbar, and $p_{O_2} = 4 \times 10^{-4}$ mbar.

TABLE 1

symbol	value	meaning
k_1	$3.14 \times 10^5\ s^{-1}\ mbar^{-1}$	impingement rate constant of CO molecules
k_2	$7.87\ s^{-1}$	desorption rate constant of CO molecules for $T = 541$ K
k_3	$265\ s^{-1}$	reaction rate constant for $T = 541$ K
k_4	$5.86 \times 10^5\ s^{-1}\ mbar^{-1}$	impingement rate constant of O_2 molecules
k_5	$1.50\ s^{-1}$	rate constant of the phase transition for $T = 541$ K
k_6	$3.00\ s^{-1}$	subsurface oxygen formation rate constant for $T = 541$ K
k_7	$2.00\ s^{-1}$	rate constant of subsurface back conversion for $T = 541$ K
s_{CO}	0.8	CO sticking coefficient at low CO coverage
$s_{O,1\times1}$	0.6	oxygen sticking coefficient on the 1×1 phase
$s_{O,1\times2}$	0.4	oxygen sticking coefficient on the 1×2 phase
u_0, δ_u	0.35, 0.05	parameters of function $f(u,s)$ for CO
s_0, δ_s	0.185, 0.05	parameters of function $f(u,s)$ for subsurface oxygen
D_x	$D_x = 80\ \mu m^2\ s^{-1}$	diffusion coefficient for CO in x direction $(1\bar{1}0)$ for $T = 541$ K
τ	0.85 s	residence time of gas in the chamber

variable, as influenced by the CO coverage and the concentration of subsurface oxygen. Equation 4 describes the formation of subsurface oxygen from the surface oxygen species and its back conversion.

The function $f(u,s)$ in eq 3 has the form

$$f(u,s) = \frac{\exp[(u - u_0)/\delta_u] + \exp[(s - s_0)/\delta_s]}{1 + \exp[(u - u_0)/\delta_u] + \exp[(s - s_0)/\delta_s]} \quad (6)$$

It describes the influence of the CO coverage and the concentration of subsurface oxygen on the structural state of the surface. The parameters u_0 and s_0 determine the threshold values above which the adsorbed CO molecules and subsurface oxygen are significantly affecting the surface structure. The parameters δ_u and δ_s specify how steep the respective thresholds are.

Equation 5 has been derived previously.[46] Details on its derivation and the interpretation of the constants are given separately in the Appendix.

In our simulations, the x axis is always along the $(1\bar{1}0)$ direction and the y axis is along the orthogonal (001) direction. One-dimensional simulations are always performed along the $(1\bar{1}0)$ direction. The oxygen diffusion is slow at the temperatures considered and is, therefore, not included in the model. In contrast to our previous work, we will not focus on temperature-dependent effects here. In the simulations, we use only a fixed temperature of $T = 541$ K, which lies approximately in the middle of the relevant temperature interval. Thus, Table 1 contains only constants of the model for this temperature as used throughout the simulations here.

To compare simulations with experimental results, provided by PEEM data, a relationship between the local PEEM image intensity and the model variables must be introduced. As discussed in previous publications,[16,18] this intensity can be approximated by a linear weighted combination

$$i = -0.3u - v + 3s \quad (7)$$

of CO and O coverages and of the subsurface oxygen concentration. Note that adsorbed CO and O decrease the image intensity, whereas subsurface oxygen leads to a strong increase of the local brightness. When simulation results are presented, we usually display only images of the composed variable i. Displaying i instead of a set of images for each variable is sufficient in most cases. The advantage of doing so is that the space−time diagram of i can be directly compared with the experimental PEEM recordings.

3.2. Wave Reflections. First, we neglect any variations of the CO partial pressure that accompany the reaction and consider a model given by eqs 1−4. This model can describe oscillatory, bistable, or excitable regimes of the reaction of interest. For the parameter values specified in Table 1, such different regimes can be established by varying the partial pressures of CO and oxygen.

In the excitable regime, oxygen waves traveling across an otherwise CO-covered surface are possible. These waves carry significant amounts of subsurface oxygen, and bright oxygen waves are observed with the PEEM. Such bright waves have been analyzed in detail in our previous publication.[18] In contrast to annihilation, which is normally found for frontal collisions of two excitation waves in activator−inhibitor models, these traveling waves may also show reflective two-into-two collisions.

An example of a reflective collision described by eqs 1−4 is presented in Figure 15. Examining the spatial concentration profiles at different stages of the collision process, we note that a significant amount of subsurface oxygen is produced and temporarily stored in the collision zone. At a later stage, this stored oxygen returns to the surface and initiates two pulses that travel back in the opposite directions from the collision zone. Effectively, the entire process can, therefore, be described as a *reflection* of two colliding waves.

From the mathematical viewpoint, the existence of reflective collisions in this model results from the presence of an additional delaying component with slow kinetics (i.e., of subsurface oxygen) that modifies the behavior found in the original system. In the absence of subsurface oxygen, the system is described by eqs 1−3. However, the oxygen coverage v is quickly adjusting to the local CO coverage u and to the phase transition variable w and can, therefore, be adiabatically eliminated. Thus, when subsurface oxygen is absent, the model can be reduced to a standard two-component activator−inhibitor system.[37] The introduction of subsurface oxygen significantly changes the behavior and brings the model into a class of multicomponent reaction−diffusion systems that have previously been investigated (see, e.g., refs 54−56) and that are known to possess special properties.

In the parameter region where reflective wave collisions are found, the system exhibits not only a uniform stationary state that corresponds to the predominantly CO-covered surface but also another uniform stationary state with a high concentration of subsurface oxygen. The latter state becomes possible because subsurface oxygen, present in sufficiently large amounts, plays a role similar to CO and stabilizes the non-reconstructed state ($w = 1$) of the surface. The collision of two waves leads to the creation of a nucleus of the other reaction state in the collision zone. This nucleus is, however, not sufficiently strong and dies out after emitting a pair of pulses.

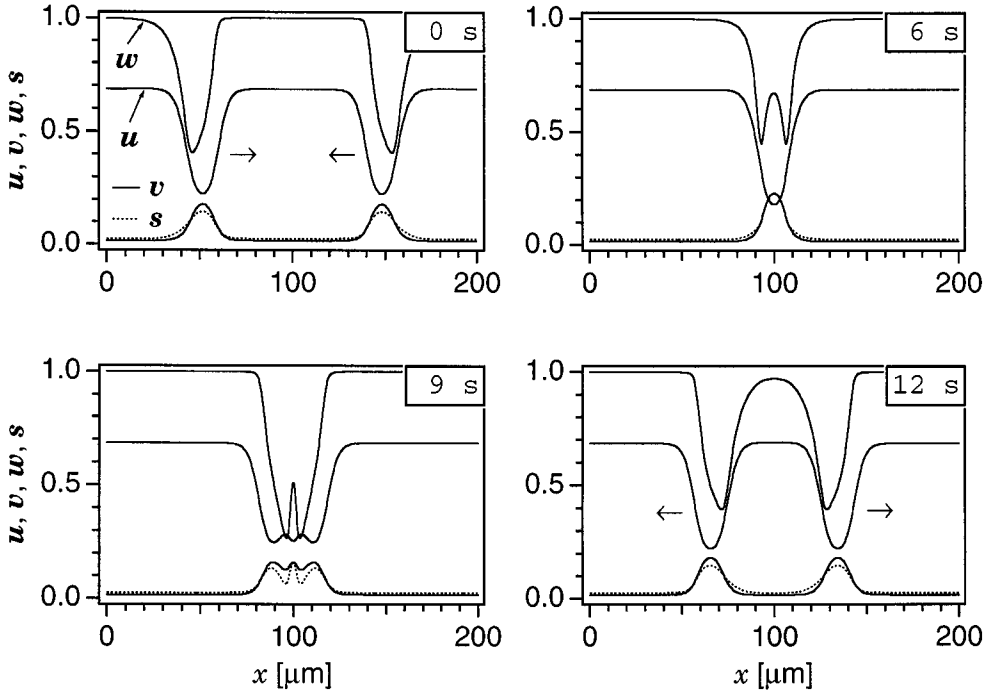

Figure 15. Simulation of a wave reflection. Profiles of the variables u (thin line), v (thin dotted line), w (thick line), and s (thick dotted line) are displayed for the four times $t = 0$, 6, 9, and 12 s. In this example, $p_{CO} = 4.142 \times 10^{-5}$ mbar, $p_{O_2} = 1.1 \times 10^{-4}$ mbar, $k_6 = 3.6\ s^{-1}$, and $k_7 = 2.11\ s^{-1}$; other parameters are given in Table 1.

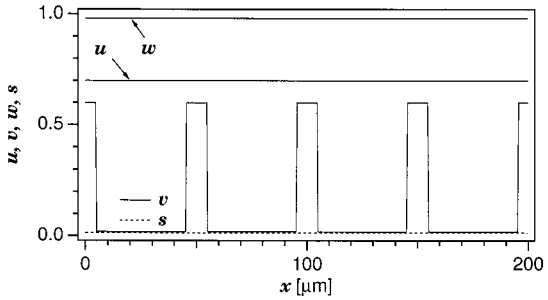

Figure 16. Initial condition for the simulation in Figure 17. The spatial distributions of the variables u, v, w, and s are shown.

When wave reflections are possible, a periodic array of bouncing waves can be created. The waves in this array repeatedly collide with their left and right neighbors and reflect from them. To produce such a pattern, we begin a simulation with the initial condition shown in Figure 16, representing a regular array of O_{ad} spots. Periodic boundary conditions are used.

Figure 17a shows the space−time diagram of the resulting pattern. Each initial O_{ad} spot gives rise to a pair of bright oxygen waves bearing subsurface oxygen. These waves collide and form metastable spots. These spots store a significant amount of subsurface oxygen. As this subsurface oxygen later returns to the surface, two new oxygen waves are produced, and the cycle is then repeated.

The graph below the space−time diagram (Figure 17b) shows the average consumption of CO by the reacting surface. The phase relation is such that whenever the surface is covered with traveling waves (e.g., at $t = 20$ s), CO consumption is maximal, whereas during the collision event (e.g., $t = 23$ s), CO consumption is minimal.

It is important to note that the spatial period of the pattern shown in Figure 17 is determined by the initial condition, that is, by the distance L between oxygen spots in Figure 16. This condition also determines the temporal period T_w of the pattern that can be roughly estimated as $T_w = L/V$, where V is the propagation velocity of the oxygen waves.

The pattern of colliding and reflecting waves, seen in Figure 17, persisted over the entire simulation. It already looks very similar to the experimentally observed patterns of standing waves (cf., e.g., Figures 5 and 11). Hence, one might think that the global feedback through the gas phase, so far neglected in the simulation, is actually not necessary for the formation of standing waves.

However, this is not true. As shown below, the pattern of colliding and reflecting waves is not robust in the absence of an external synchronizing force. It is easily destroyed even by weak defects dispersed in the medium.

Despite careful preparation, single crystal surfaces usually still contain a significant number of defects that modify the local reaction properties. Some of these defects are extended (like the defect in Figure 1), but most of them are so small that they are not resolved by the PEEM. Various kinds of defects with different properties are possible.

In our simulations, we model a defect by assuming that CO sticking is slightly enhanced at defect locations. The defects are randomly distributed in the medium and are produced by a locally varying CO sticking coefficient s_{CO}, as shown in Figure 18b. In the absence of a reaction, these defects lead to slight local variations in the CO coverage, as shown in Figure 18c.

We start the simulation with the same initial conditions as in Figure 16. The space−time diagram of the developing pattern is shown in Figure 18a. We see that, during the first few collision cycles, the pattern remains similar to that shown in Figure 17. However, irregularities in the pattern already begin to develop. Because of random variations in the local properties of the medium, some metastable spots live longer and send waves later than other such objects. Thus, the periodicity of the pattern becomes destroyed. In addition to reflective two-into-two collisions (such as the collision marked by 1), fusion of two colliding waves (marked by 3) and mutual annihilation (marked by 2) are also found. The annihilations take place when a

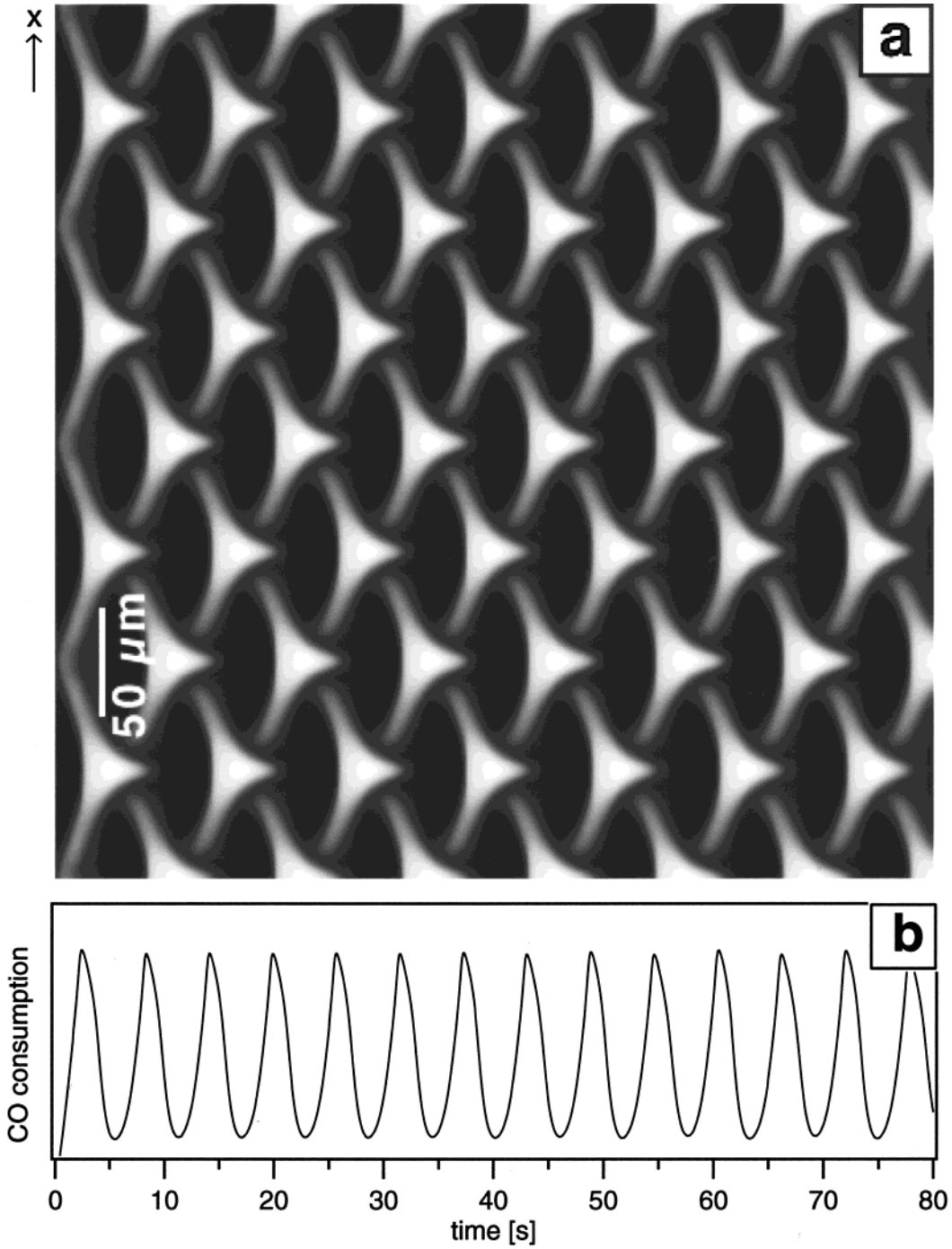

Figure 17. (a) Space−time diagram of the calculated PEEM intensity in a one-dimensional simulation of a pattern produced by repeated reflecting wave collisions. (b) Computed time dependence of the CO consumption in this pattern. The time interval shown is 80 s; the system length is 200 μm. Same parameters as in Figure 15.

collision occurs at a location with a higher CO sticking coefficient and, thus, a lower excitability for oxygen waves.

Because some of the collisions do not conserve the number of waves, the pattern becomes more sparse, and eventually the wave activity dies out. At the end of the simulation, the medium is found in the stationary state with the prevailing CO coverage. Thus, we see that reflective wave collisions alone cannot explain the persistence of standing waves seen in the experiments.

3.3. Standing Waves Generated by External Forcing. In this section, we show that, when periodic external forcing of the CO partial pressure is applied, standing waves develop from arbitrary, random initial conditions. These waves are stable with respect to the presence of even large defects.

The external forcing is introduced by assuming that the CO supply flux though the CO gas inlet j_{inlet} is periodically modulated with time. As shown in the Appendix (eq 12), this is equivalent to assuming that the constant p^0_{CO} in eq 5 varies periodically with time, specifically,

$$p_{\mathrm{CO}}(t) = p^{\mathrm{m}}_{\mathrm{CO}} + p^{\mathrm{a}}_{\mathrm{CO}} \sin\left(\frac{2\pi t}{T_{\mathrm{mod}}}\right) \tag{8}$$

The actual CO partial pressure, $p_{\mathrm{CO}}(t)$, in the chamber is determined by eq 5. It adjusts to variations of the CO supply flux with a certain delay that is determined by the characteristic residence time $\tau = 1/\gamma$ of the reaction chamber. We neglect

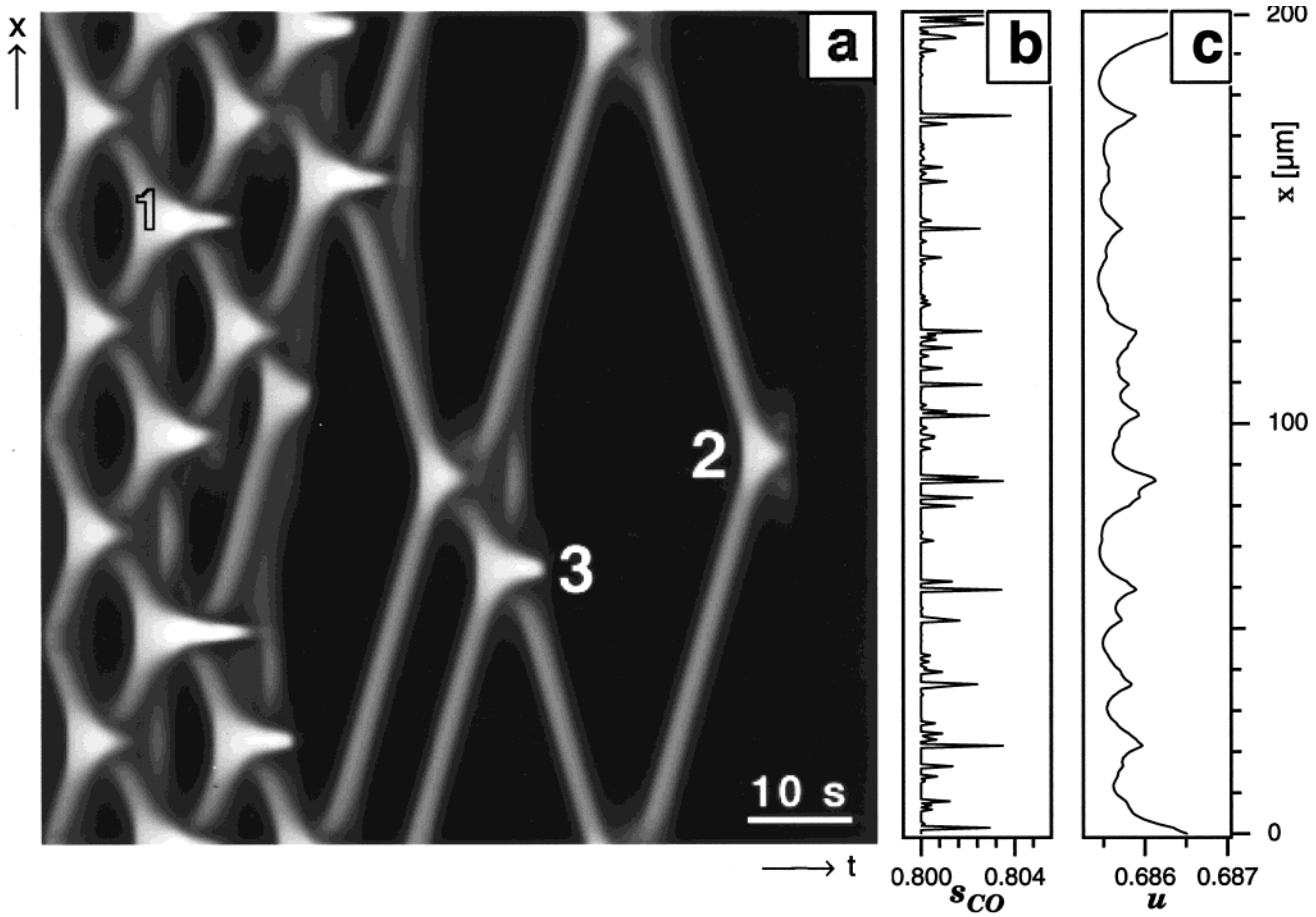

Figure 18. Simulation with the same parameters as in Figure 15, but with randomly distributed surface defects. The spatial distribution of the CO sticking coefficient (b) is plotted to the right of the space−time diagram (a). Plot (c) shows the spatial distribution of CO coverage resulting from this defect distribution in the stationary CO-covered state.

here the effect of the reaction on the CO partial pressure by setting $\chi = 0$ in eq 5.

The initial condition for the simulations was constructed by assigning independent random values from the interval [0,1] to the variables u, v, and w at every grid point. Subsurface oxygen was initially absent ($s = 0$). The modulation period was $T_{mod} = 3.5$ s, and the forcing parameters were chosen as $p^{m}_{CO} = 4.07 \times 10^{-5}$ mbar and $p^{a}_{CO} = 7 \times 10^{-7}$ mbar, corresponding to the relative modulation amplitude of 1.7%. Periodic boundary conditions were used.

Figure 19 displays the resulting space−time diagram of the developing standing wave pattern. The plot below this diagram shows the corresponding temporal variation of the CO pressure in the chamber. We see that, during the initial time interval of about 2 s after the beginning of the simulation, the pattern remains random and is essentially determined by the initial distribution. However, at the end of the first modulation period, a seed of a standing wave pattern suddenly appears at a certain location. Later, this seed gradually spreads until the whole medium is covered by a standing wave pattern.

Additional simulations, in which the modulation periods were varied, were performed. We have found that a pattern of standing waves emerges from a random initial distribution for modulation periods in the range from 2.6 to 4.6 s. The pattern includes one or two more collision zones in the case of a faster modulation and one less node for the slower modulation. Hence, the spatial period of the developing standing wave is also controlled by the external forcing. It should be noted that, because periodic boundary conditions were used in this simulation series, the total length of the system was always equal to an integer number of spatial periods of the standing wave, and thus, not any arbitrary spatial period was allowed.

This limitation is somewhat artificial. In a real experiment, the linear size of the reacting surface is many orders of magnitude larger than the spatial period of the standing waves, and furthermore, the pattern of standing waves typically occupies only part of the entire catalyst surface. Therefore, the actual boundary effects should not be important in determining the properties of this pattern.

To eliminate the restrictive effect of the boundary condition, special simulations with nonuniform media were performed. Inside a certain relatively large region, the CO sticking coefficient was increased to a level such that wave propagation was no longer possible there. This region, therefore, provided a "sink" for propagating waves that were softly dying when entering this area.

The simulation was started with the same random initial conditions as were used for Figure 19. The modulation period was gradually increased during this simulation from 3.0 to 4.2 s within the time interval of 450 s. Figure 20 shows the space−time diagram of the standing wave pattern obtained in this simulation (for convenience, this diagram is cut into two separate segments placed one under another).

We see that the pattern does not develop into the bottom region where the effective excitability of the medium is low because of a higher CO sticking coefficient. This region remains in the predominantly CO-covered state. A very interesting behavior is found near the boundary of this modified region.

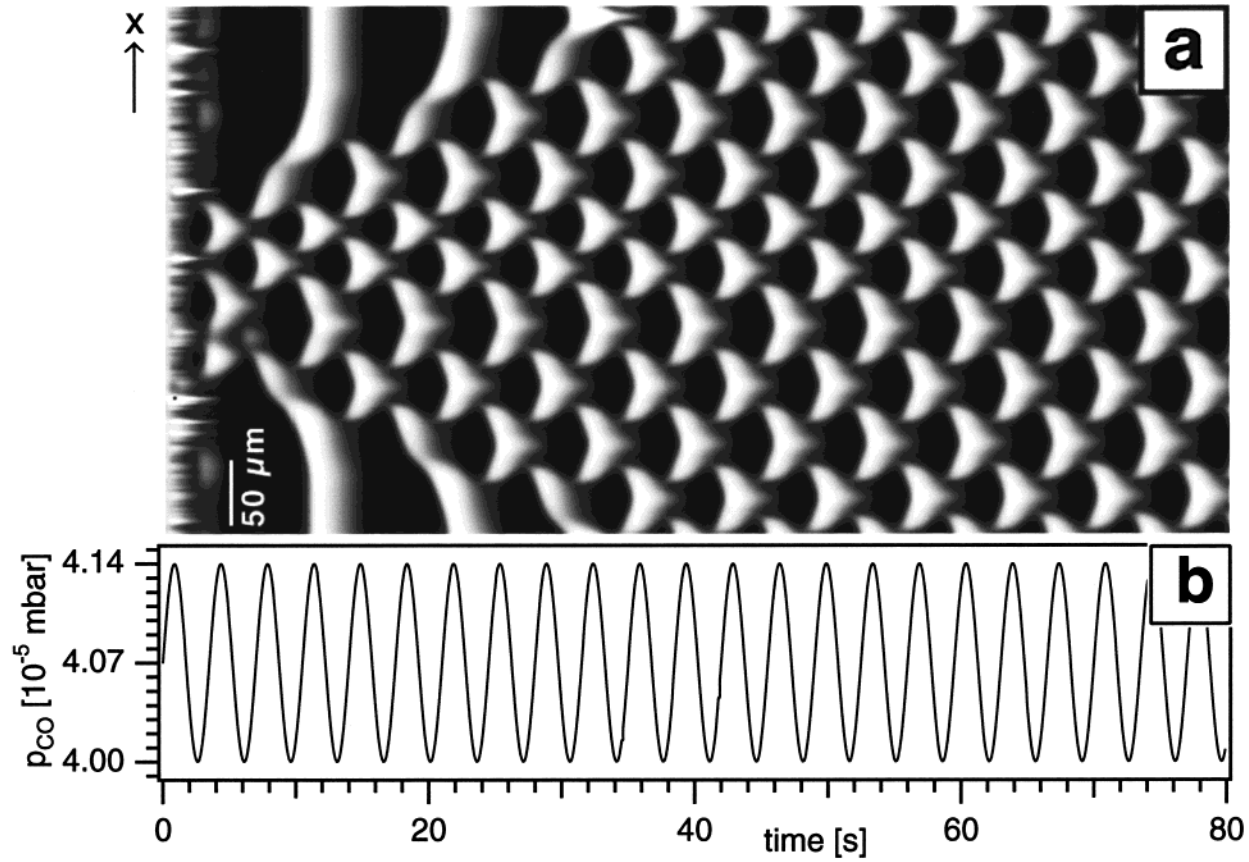

Figure 19. Development of standing waves under external forcing from random initial conditions. (a) Space−time diagram of the calculated PEEM intensity and (b) time dependence of the CO partial pressure in external forcing are shown. The oxygen partial pressure is $p_{O_2} = 1.1 \times 10^{-4}$ mbar; other parameters are given in Table 1. The system length is 400 μm.

The waves, emitted by the pattern, die out as they penetrate into the modified surface area. Hence, no reflections take place here. Despite their absence, the pattern of standing waves is persistent. This effect must be attributed to external forcing. Indeed, in the absence of external forcing, the pattern would start to shrink and would eventually disappear.

Moreover, we can observe in Figure 20 that the spatial period gradually adjusts itself to the continuous increase of the temporal period of external forcing. The total number of nodes varies from 11 at the beginning of simulation to ca. 7 at its end. This corresponds approximately to the increase in the modulation period from 3.0 to 4.2 s. It can also be noted that, closer to the simulation end, the pattern has already started to show dynamical instabilities that would destroy the pattern if the modulation period were further increased.

Hence, we can conclude that periodic external forcing can induce standing waves that remain stable even with respect to strong surface perturbations, such as the presence of a modified nonexcitable region.

3.4. Intrinsic Forcing of Standing Waves. So far, we have neglected the influence of the reaction itself on the partial pressures of reactants. However, this influence, described by eq 5, is always present under experimental conditions and provides a global feedback mechanism. Effectively, the reaction is generating a forcing signal that acts back on it. This intrinsic forcing might play a role similar to that played by the external forcing studied in the previous section and might stabilize the standing wave pattern.

Simulations were performed in which the gas-phase coupling, described by eq 5, was taken into account. In the first series of such simulations, we assumed that the standing waves occupied the entire available medium. The results of all of these simulations were negative. We have found that a standing wave pattern never spontaneously developed out of random initial perturbations. Moreover, even if such a pattern is taken as the initial condition, even a weak gas-phase feedback, such as a CO partial-pressure variation of only 0.1%, would quickly destroy the pattern and lead to a stationary state of the reaction.

The effect can be rationalized by analyzing the CO consumption by a standing wave pattern (Figure 17b). We notice that the CO consumption is low when the colliding waves have merged to form metastable spots. The lower CO consumption implies, however, a higher partial pressure of CO. Hence, when the subsurface oxygen spots are formed, the CO partial pressure rises as a result of the gas-phase feedback. However, this effect is exactly opposite to what is needed to stabilize the standing wave pattern. Indeed, an examination of Figure 19 reveals that, when external forcing through periodic variation of the CO pressure is applied, the minima of p_{CO} correspond to time intervals when spots are observed.

Thus, the relative phase of self-modulation produced by the standing wave pattern is shifted by one-half temporal period with respect to what is needed to enhance and stabilize such a pattern. Therefore, self-supporting standing waves that occupy the entire medium are not possible in the model.

In analyzing the experimental data, however, we noted in section 2.2 that standing waves were never seen in the experiments to occupy the entire catalytic surface. Typically, they occupied only part of the area, while the rest of the surface was found in a state of spatially uniform synchronous kinetic oscillations. The nonuniformity of the reaction regime might

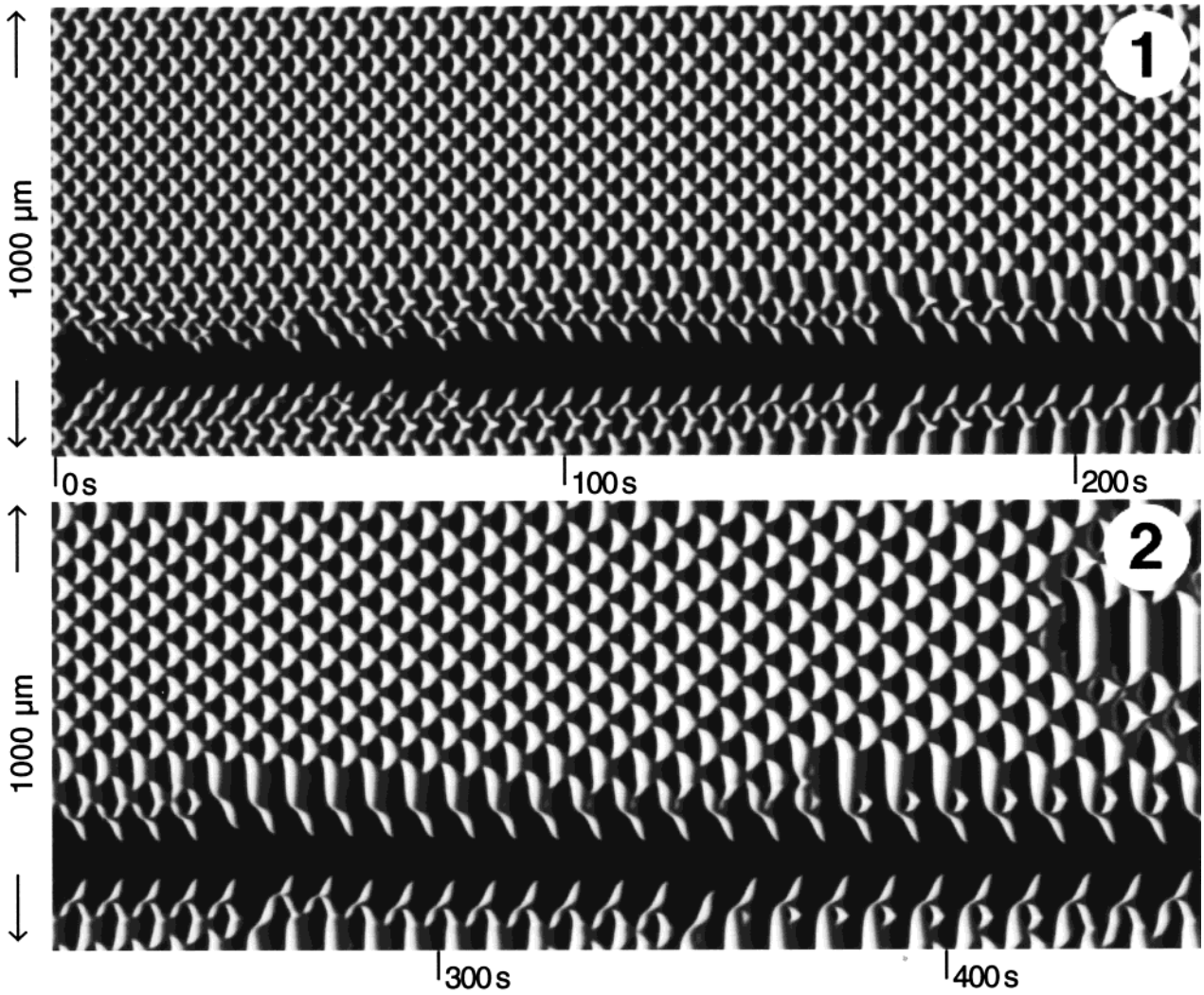

Figure 20. Evolution of the standing wave pattern during the gradual increase of the external forcing period from 3.0 to 4.2 s over the total time of 450 s. The space−time diagram of the calculated PEEM intensity is cut into two segments (1 and 2), each of length 225 s, that are placed vertically one under another. The system length is 1000 μm. The lower region of the system, where waves are absent, has a CO sticking coefficient enhanced by 2%. Same reaction parameters as in Figure 19.

be related to the fact that the local surface properties have been slightly modified, either by the use of the same sample in previous experiments or even by the PEEM itself inside its observation window, as will be further outlined in the Appendix.

If synchronous oscillations are taking place across a relatively large fraction of the surface, however, they cause a modulation of the CO partial pressure that effects a periodic forcing on other surface areas where the parameters are slightly different and, instead of undergoing oscillations, the surface is found in the excitable stationary state. Such intrinsic forcing may then induce and stabilize standing waves in these regions.

To test this conjecture, simulations were performed in which modulation of the CO partial pressure was produced by a uniformly oscillating large part of the surface. The computed kinetic oscillations are shown in Figure 21. Their profile is not harmonic. Note that significant amounts of subsurface oxygen are produced in such oscillations during the cycle stage in which the surface is oxygen-covered.

Figure 22b shows how the CO partial pressure in the chamber varies if the oscillatory reaction shown in Figure 21 consumes part of the CO from the gas phase. This time dependence was computed using eq 5 with realistic values for γ and χ, where only the contribution from the surface area involved in uniform oscillations was taken into account. Contributions to the CO consumption that would arise from the part of the surface covered with standing waves were neglected.

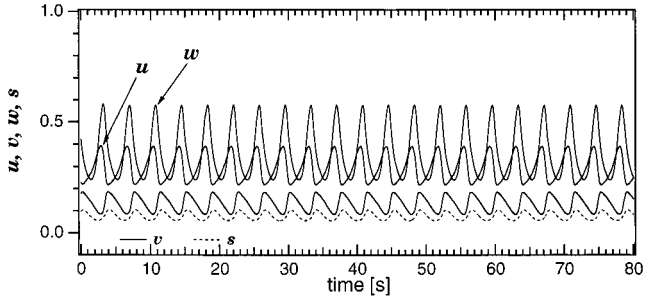

Figure 21. Uniform kinetic oscillations for $p^0_{CO} = 5.245 \times 10^{-5}$ mbar, $p_{O_2} = 1.1 \times 10^{-4}$ mbar, $s_{CO} = 0.99$, $\gamma = 0.59$ s^{-1}, and $\chi = 7 \times 10^{-7}$ mbar/m^2; other parameters are given in Table 1. The temporal evolution of p_{CO} is shown in Figure 22b.

Figure 22a shows the space−time diagram of a one-dimensional simulation in which the intrinsic forcing has been applied to the medium in the excitable stationary state. A random defect distribution was introduced in this simulation by a local variation of the CO sticking coefficient by 1%, so that the local excitability for oxygen waves is slightly enhanced at some sparsely distributed locations. The p_{CO} modulation corresponds to the oscillations in the uniformly oscillating area and is

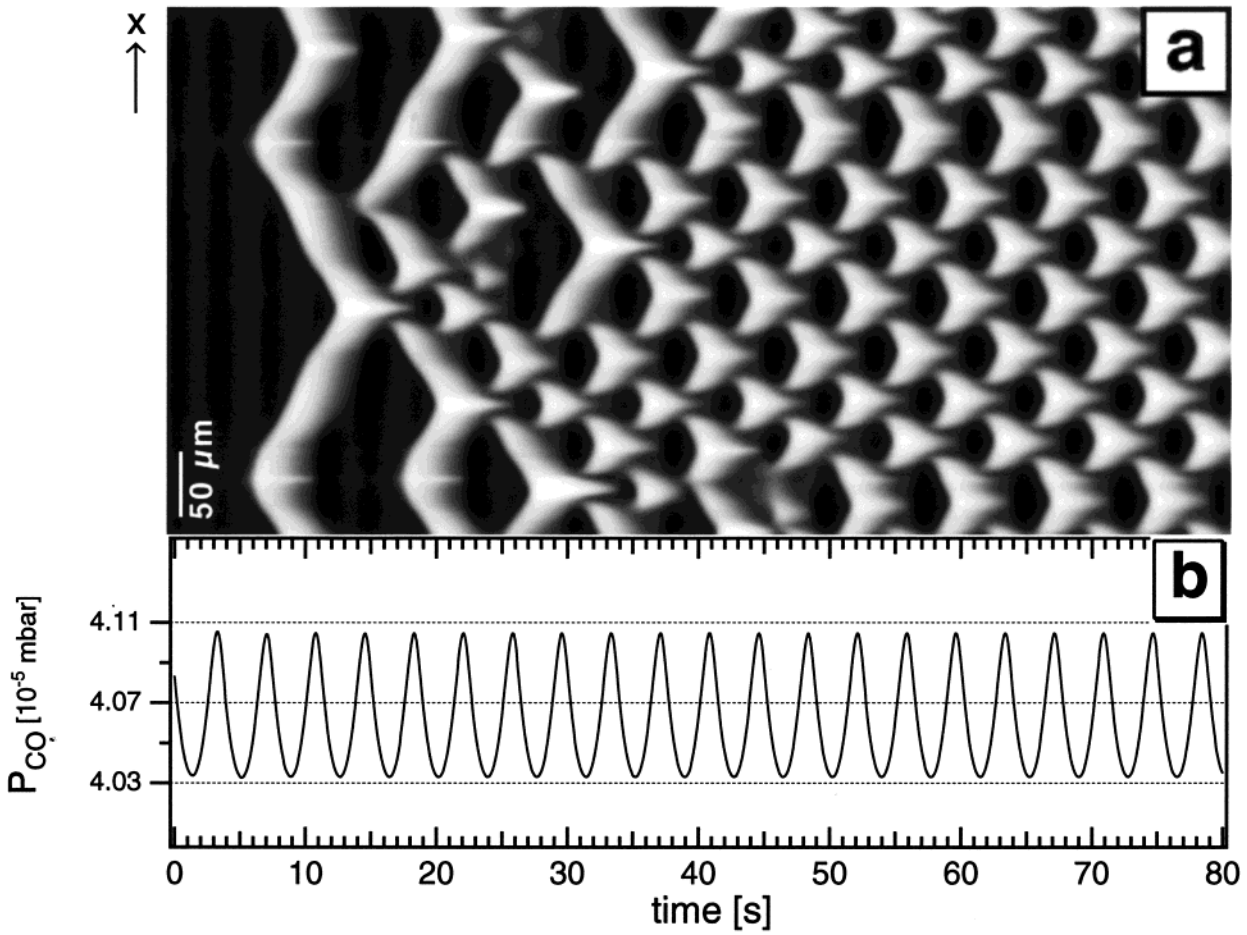

Figure 22. Development of standing waves under intrinsic forcing by the oscillating surface area. (a) Space−time diagram of the calculated PEEM intensity and (b) time dependence of the CO partial pressure are displayed. The temporal modulation of the CO pressure is produced by kinetic oscillations in another part of the surface (not shown), with the parameters given in Figure 21. The system length is 400 μm, and $p_{O_2} = 1.1 \times 10^{-4}$ mbar; other parameters are given in Table 1.

characterized by a mean value of 4.07×10^{-5} mbar and an amplitude of 1%. Periodic boundary conditions were used.

We see that the intrinsic periodic forcing induces small-amplitude-driven oscillations in the medium whose state remains practically uniform within the first 8 s. Then suddenly, two regions become activated, and two pairs of waves are nucleated. Subsequent collisions of the waves initiate a standing wave pattern that rapidly spreads to occupy the total available part of the medium. The corresponding variation of the CO partial pressure in the chamber is shown below in Figure 22b.

Two-dimensional simulations that included intrinsic forcing by an independently oscillating homogeneous domain, as discussed previously, were also performed. Figure 23 displays several consecutive frames for such a simulation. Figure 24 shows the corresponding space−time diagram for the evolution along the central horizontal cross section in the images in Figure 23. The same kind of defect distribution as in Figure 22 was used here. Periodic boundary conditions in both directions were applied.

We see that, under the influence of intrinsic forcing, produced by the uniformly oscillating part of the surface (not shown in the figures), the two strongest defects start to emit waves (frame 1). These waves collide and form a bright vertical stripe in the collision zone (frame 2). This stripe splits into two parts that move in opposite directions away from the collision zone. Subsequent reflective collisions between these waves and the active defects lead, through a complex transient process (frames 3 and 4), to suppression of the defect activity (frame 5) and finally to the appearance of a regular pattern of standing waves that occupies the entire available medium (frame 6). This pattern represents an array of linear stripes that periodically split and collide with their neighbors. The computer video of this simulation is available on the World Wide Web at http://www.fhi-berlin.mpg.de/~complsys. (See also Supporting Information.)

The space−time diagram of the initial stage of this process (Figure 24) is similar to the corresponding diagram for a one-dimensional medium (Figure 22). However, the transient is much longer in two dimensions and takes approximately 70 forcing periods.

4. Discussion and Conclusions

We have presented the results of a detailed experimental and theoretical study of a particular type of spatio-temporal patterns that were so far observed only in surface chemical reactions. Our experiments suggest that the formation of subsurface oxygen plays an important role in this phenomenon. The increased formation of subsurface oxygen in the collision zone of two colliding oxygen waves and its subsequent slow release back to the surface explain why annihilation is replaced by reflections of excitation waves in the parameter region where standing wave patterns are observed.

When a periodic wave array is initially created, repeated wave reflections of a wave from its neighbors cause bouncing of waves inside the array and, thus, produce a structure that already

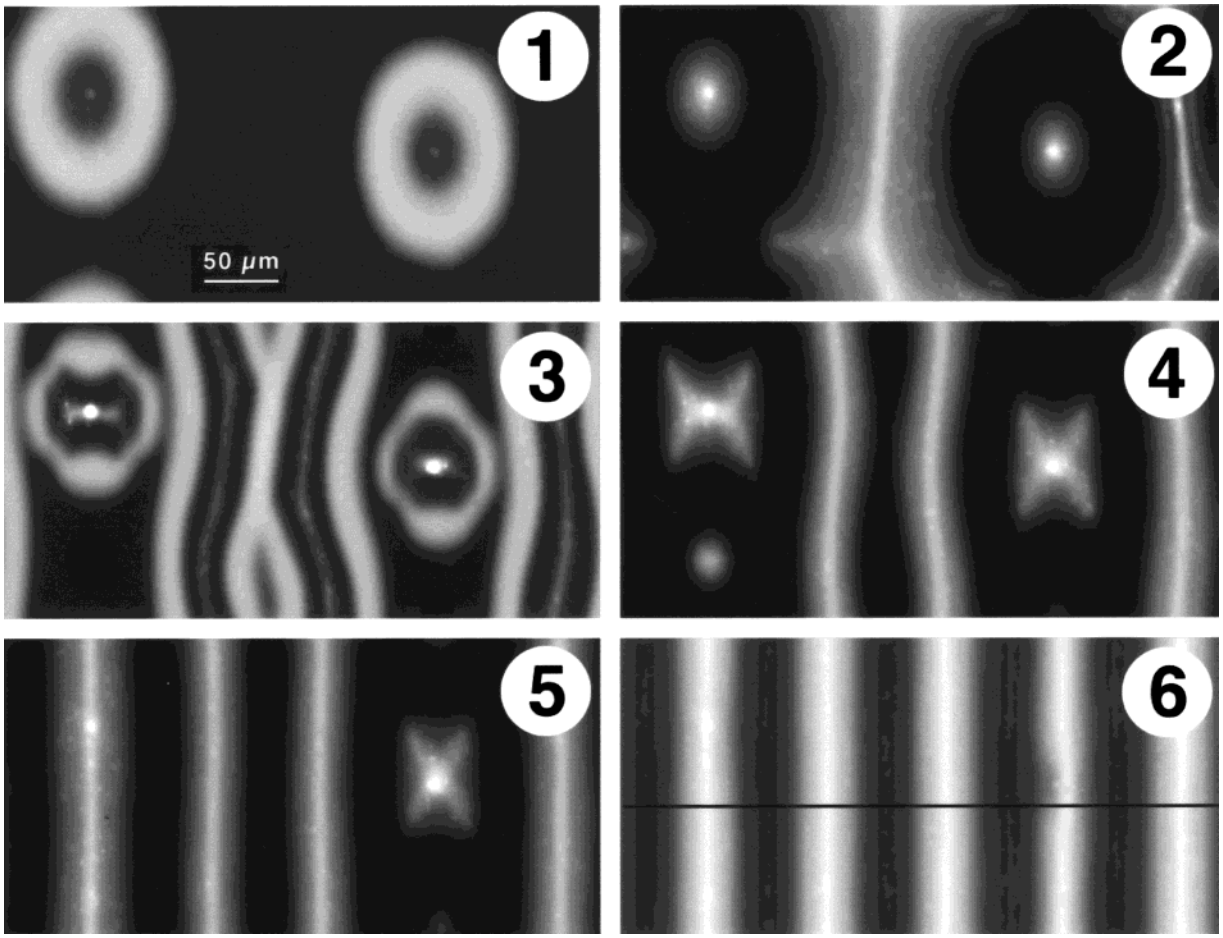

Figure 23. Snapshots of a two-dimensional simulation for a system of size 400 μm × 200 μm under forcing by a uniformly oscillating region (not shown). Times in frames 1−6 are t = 10, 16.2, 32.6, 45.6, 175.8, and 210.8 s, respectively. Same forcing conditions and parameter values as in Figures 21 and 22. Diffusion anisotropy is 0.5.

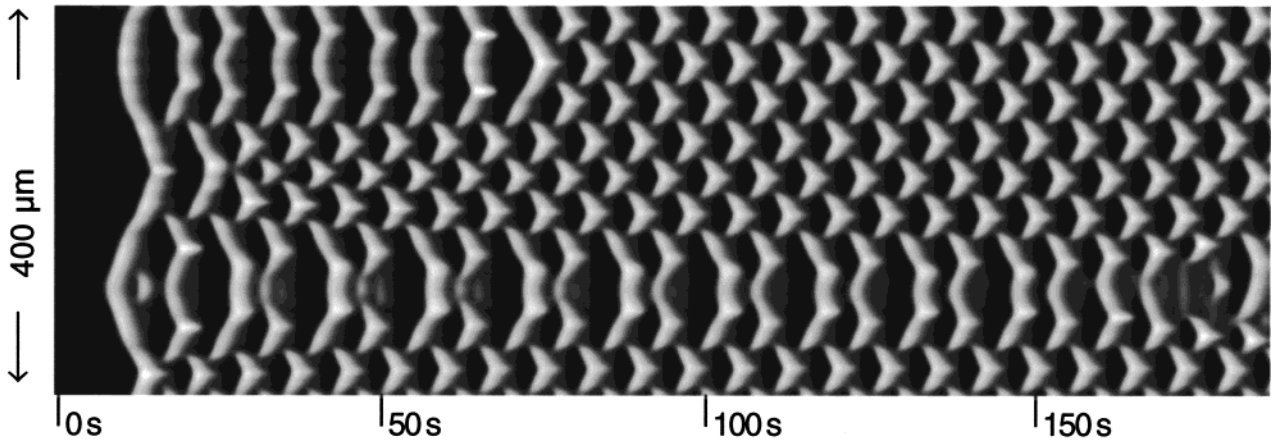

Figure 24. Space−time diagram of the developing standing wave pattern along the cross section indicated by a horizontal black line in Figure 23. The time interval shown is 186 s; the system length is 400 μm.

looks like a pattern of standing waves. However, the effect of reflections alone cannot account for the observed properties of standing waves.

If a standing wave pattern were based solely on the local effect of wave collisions, its spatial and temporal period would be essentially arbitrary, that is, it would be determined by the initial spacing of waves in the array. This pattern would be very unstable and would easily be destroyed even by small surface inhomogeneities and defects. Moreover, if standing waves were to occupy several disconnected areas on the surface, they would generally be characterized by different spatial and temporal periods.

The standing waves seen in the experiments were stable and were sometimes observed even over hours. They were perfectly synchronized and had the same spatial and temporal periods, even in distant parts of the surface that were separated by regions with uniform oscillations. Apparently, such kinetic oscillations are important for the persistence of standing waves. Indeed,

whenever they stopped, the pattern of standing waves immediately broke down into a set of traveling wave fragments (Figure 6).

Interactions between distant parts of the surface are indeed mediated through gas-phase coupling. The local reaction consumes CO and O_2 from the gas phase. Because of the applied partial pressures, the mean free path of molecules in our experimental chamber was comparable to or even larger than its linear size (i.e., ≥ 10 cm). Thus, molecular motion led to rapid mixing and equilibration of the partial pressures of gaseous reactants on a time scale of about 10^{-4} s, which was determined by the average molecular speed of 10^3 m/s and the dimension of 10^{-1} m of the reaction chamber. Consequently, the processes taking place in one area of the reactive surface can almost instantaneously influence the reaction course in other surface areas.

On the other hand, it can be noted that the reaction properties were not perfectly uniform in the experiments in which standing waves were observed. The crystal surface may have been locally modified by previous experiments, producing certain amounts of roughening. Hence, the reaction conditions might be different across the surface, and some parts of the surface might have been in the regime of kinetic oscillations, whereas its other parts were characterized by excitable kinetics.

The analysis of experimental data suggests that kinetic oscillations, taking place in specific surface areas, can lead to small periodic variations of the CO partial pressure in the chamber that act as intrinsic forcing applied to the reaction on the rest of the surface. This suggestion is supported by the experiments in which external forcing of the reaction was realized by periodic modulation of the CO supply through the CO gas inlet. We have seen that such modulation can easily synchronize standing wave patterns and change their temporal periods (Figures 12 and 13). Importantly, the induced variation of the partial CO pressure in these experiments was not much higher than the intrinsic variation of this pressure that is due to gas coupling under oscillatory conditions.

In a further experiment, we were able to simultaneously record the evolving PEEM image of the reaction and the current CO partial pressure, as measured by means of a quadrupole spectrometer (QMS). In this experiment, both uniform oscillations and a pattern of standing waves were simultaneously observed in different parts of the PEEM window (Figure 14). We have found that the recorded QMS signal yielded the same phase relation as was observed for entrained standing waves under the conditions of external forcing (Figure 13).

Numerical simulations of standing waves for the catalytic reaction under consideration have been performed. These simulations were based on the previously developed kinetic model for the CO oxidation reaction on Pt(110), which was extended to include the effects of subsurface oxygen. The exact model parameters were determined in our earlier publication,[18] in which they were deduced from independent experimental data on conversion of oxygen islands. The same set of parameters was used here to simulate the development of standing waves in this system. Additionally, we included in our theoretical description gas-phase coupling that occurred during the reaction (eq 5). Its parameters were also quantitatively estimated (see the Appendix).

The simulations have shown that uniform kinetic oscillations in one surface area can indeed induce, through gas-phase coupling, the development of standing waves in another part of the surface (Figures 22−24). In a manner similar to the experimental observations (Figure 8), the standing wave pattern develops from colliding oxygen waves initiated by randomly distributed surface defects. The developing pattern of standing waves has a form of linear stripes that periodically split and collide with their neighbors (Figure 23), as was indeed observed in the experiments. The simulated PEEM intensity profiles closely resemble the experimental images.

Although we did not attempt to reach quantitative agreement with experiment and although the reaction parameters were not identical to those used in the experiment, we note that the characteristic wavelengths and temporal period of the simulated standing waves are of the same order of magnitude as those in the experiments.

Furthermore, we have studied theoretically the behavior of standing waves under external forcing. In agreement with the experimental data, the entrainment effect was found for standing waves in a relatively large interval of the temporal period of external forcing (Figure 20).

Our simulations show that, if a standing wave pattern is initially created in the absence of external forcing, it rapidly becomes destroyed, being transformed into a set of traveling waves if the reactive surface is microscopically inhomogeneous and contains many small defects (Figure 18). This result agrees with the corresponding experimental observation that, when kinetic oscillations disappear, the standing wave disintegrates into a set of traveling waves (Figure 6).

Hence, we conclude that the model can successfully reproduce the principal observed properties of standing waves in the CO oxidation reaction on Pt(110).

One of the predictions of this model is that autonomous self-supporting standing waves that occupy the entire surface are not possible. Standing waves appear as a consequence of uniform oscillations occurring in a separate region of the surface. We cannot exclude the possibility that, when other processes such as facetting (see below) and lateral interactions between adsorbed molecules are properly taken into account, this prediction is altered, and autonomous standing waves might be found. The available experimental observations seem, however, to confirm our conclusion, as standing waves have so far never been seen to cover the entire sample surface. When standing waves were observed, uniformly oscillating regions were usually also found on the surface.

In our studies, we could not reproduce the period-doubling instability of standing waves that was seen in the experiment (Figures 3 and 4). Moreover, a slow drift of the reaction regime was sometimes found in the experiments when standing waves were observed (cf. Figures 2 and 6). This indicates a modification of the surface that proceeds on a relatively large time scale.

In this context, the phenomenon of surface facetting and roughening should be mentioned.[12,13,57,58] The gradual change of oscillation frequency observed in Figure 6 has the same tendency as was observed for the Pt(110) surface undergoing gradual facetting. The PEEM technique does not, however, give any direct evidence for facetting or roughening, and we could not analyze whether either process occurred in the experimental situation. This aspect should be further investigated.

Acknowledgment. The authors acknowledge financial support from Deutsche Forschungsgemeinschaft (Germany) in the framework of Sonderforschungsbereich 555 “Complex Nonlinear Processes”.

Appendix

In this Appendix, we derive dynamic eq 5 that governs evolution of the CO partial pressure in the reaction chamber,

and we determine its parameters corresponding to our experimental conditions. The derivation generally follows the previous publication.[46]

We assume that the CO kinetics in the chamber is characterized by the laws of an ideal gas (see, however, a brief discussion at the end of this Appendix) and start from the thermodynamic equation of state for ideal gases, namely

$$N_{CO} = \frac{p_{CO} V_{Ch}}{k_B T_0} \tag{9}$$

where N_{CO} is the number of CO molecules found in the chamber of volume V_{Ch} at pressure p_{CO}. Here, temperature T_0 is the gas temperature in the chamber, and k_B is the Boltzmann constant. The number N_{CO} changes with time according to

$$\frac{dN_{CO}}{dt} = j_{inlet} - j_{pump} - j_{reaction} \tag{10}$$

Here, j_{inlet} is the incoming flux of CO molecules into the chamber, j_{pump} is the flux of these molecules pumped out of the chamber, and $j_{reaction}$ is the rate of consumption of CO molecules in the surface reaction.

The flux j_{pump} can be estimated as

$$j_{pump} = \gamma \frac{p_{CO} V_{Ch}}{k_B T_0} \tag{11}$$

where the coefficient γ represents the fraction of CO molecules in the chamber that are evacuated per unit time by the vacuum pump. Note that the inverse of this coefficient yields the characteristic residence time $\tau = 1/\gamma$ of CO molecules in the chamber in the absence of any reaction. It is convenient to write the incoming flux in a similar form

$$j_{inlet} = \gamma \frac{p^0_{CO} V_{Ch}}{k_B T_0} \tag{12}$$

thus defining the new parameter p^0_{CO}. Finally, the total consumption rate of CO molecules in the reaction is given by

$$j_{reaction} = \rho \int_A [k_1 s_{CO} p_{CO} (1 - u^3) - k_2 u]\, da \tag{13}$$

Here, we have taken into account the fact that, because of the material balance, the consumption rate is equal to the difference of adsorption and desorption fluxes. The integration is performed over the entire surface area A. The coefficient ρ is the number of adsorption sites per unit area and is 9.2×10^{18} m^{-2}.

Dividing both parts of eq 10 by $V_{Ch}/k_B T$, we obtain the evolution eq 5, in which the gas-phase coupling coefficient is given by

$$\chi = \frac{\rho k_B T_0}{V_{Ch}} \tag{14}$$

Examining eq 5, we also note that the parameter p^0_{CO}, defined by eq 12, gives the steady-state CO partial pressure in the pumped chamber in the absence of any reaction. The residence time $\tau = 1/\gamma$ specifies a characteristic time needed to reach this stage.

For our PEEM experiments, described in this paper, the chamber had the volume $V_{Ch} = 0.06$ m^3, and the gas in the chamber was at room temperature $T_0 = 300$ K. Thus, the gas-coupling coefficient was $\chi = 0.63$ mbar/m^2. This value can be used to calculate the theoretical pressure one would obtain if one monolayer of CO molecules initially adsorbed on the surface area of the crystal ($A = 7.85 \times 10^{-5}$ m^2) were fully transferred into the empty volume of the chamber. This value is 5×10^{-7} mbar. The coefficient γ can be roughly evaluated as the ratio $\gamma = j_p/V_{Ch}$ of the volume j_p that is pumped out per unit time to the total volume V_{Ch} of the chamber. For the technical data given for our pump, $j_p = 360$ L/s, this ratio yields $\gamma \approx 6$ s^{-1}, and hence, the residence time $\tau = 0.2$ s. However, mounting of the turbomolecular pump and regulation with the respective valve may increase the chamber residence time from 0.2 up to 1 s and more.

In principle, a similar evolution equation can be derived for the variation of the oxygen partial pressure in the chamber. The feedback via the oxygen partial pressure is, however, much less pronounced, and therefore, we do not take it into account. Each O_2 molecule carries two oxygen atoms that are available for the reaction, and the required pressure of O_2 is typically at least two times larger than the CO pressure. Thus, the consumption of oxygen molecules produces less than one-quarter of the effect on the corresponding partial pressure than does the consumption of CO.

The above analysis was performed assuming that the gas inside the chamber is described by the standard equations of gas kinetics. It should be remembered, however, that these equations are only valid when the mean free path of gas molecules in a vessel is much shorter than the linear dimensions of the vessel. In the ballistic regime, characterized by the opposite relationship between the two lengths, the gas kinetics will be dominated by collisions of molecules with the walls of the vessel. An important property of such a ballistic regime is that the partial pressures of gases in adjoining vessels with different wall temperatures are not equal.

In our experiments, the gas parameters in the chamber were at a crossover from the standard gas kinetics to the ballistic regime. When PEEM measurements were recorded, the imaged surface area of the crystal was separated by only a narrow gap from the PEEM objective. Because the crystal was heated much above the room temperature, at which the walls of the reaction chamber were kept, the kinetic conditions in this narrow gap region might be different, and a certain increase in the partial pressures of reactants could actually occur within the PEEM observation window. Quantitative estimates of the resulting corrections are, however, difficult and cannot be presented here.

Supporting Information Available: Three QuickTime movies showing PEEM images of the development and oscillations of standing wave patterns and one QuickTime movie showing a simulation of the development of an oscillating stripe pattern (standing waves) from uniform initial conditions. This material is available free of charge via the Internet at http://pubs.acs.org.

References and Notes

(1) Winfree, A. T. *Science* **1972**, *175*, 634.

(2) Zhabotinsky, A. M.; Zaikin, A. N. *Nature* **1970**, *255*, 535.

(3) Belousov, B. P. A Periodic Reaction and Its Mechanism (1951, from his archives). In *Oscillations and Travelling Waves in Chemical Systems*; Fields, R. J., Burger, M., Eds.; Wiley: New York, 1985; p 605.

(4) Imbihl, R.; Ertl, G. *Chem. Rev.* **1995**, *95*, 697.

(5) Jakubith, S.; Rotermund, H. H.; Engel, W.; Oertzen, A. v.; Ertl, G. *Phys. Rev. Lett.* **1990**, *65*, 3013.

(6) Rotermund, H. H.; Engel, W.; Jakubith, S.; Oertzen, A. v.; Ertl, G. *Ultramicroscopy* **1991**, *36*, 164.

(7) Ehsasi, M.; Frank, O.; Block, J. H.; Christmann, K. *Chem. Phys. Lett.* **1990**, *165*, 115.

(8) Middya, U.; Luss, D.; Sheintuch, M. *J. Chem. Phys.* **1994**, *100*, 6386.
(9) Middya, U.; Luss, D.; Sheintuch, M. *J. Chem. Phys.* **1994**, *101*, 4688.
(10) Luss, D. *Ind. Eng. Chem. Res.* **1997**, *36*, 2931.
(11) Eiswirth, M.; Ertl, G. *Surf. Sci.* **1986**, *177*, 90.
(12) Ladas, S.; Imbihl, R.; Ertl, G. *Surf. Sci.* **1988**, *197*, 153.
(13) Ladas, S.; Imbihl, R.; Ertl, G. *Surf. Sci.* **1988**, *198*, 42.
(14) Rotermund, H. H.; Lauterbach, J.; Haas, G. *Appl. Phys. A* **1993**, *57*, 507.
(15) Lauterbach, J.; Asakura, K.; Rotermund, H. H. *Surf. Sci.* **1994**, *313*, 52.
(16) Oertzen, A. v.; Mikhailov, A. S.; Rotermund, H. H.; Ertl, G. *Surf. Sci.* **1996**, *350*, 259.
(17) Rotermund, H. H. *Surf. Sci. Rep.* **1997**, *29* (7/8), 265.
(18) Oertzen, A. v.; Mikhailov, A. S.; Rotermund, H. H.; Ertl, G. *J. Phys. Chem. B* **1998**, *102*, 4966.
(19) Engel, T.; Ertl, G. *Adv. Catal.* **1979**, *28*, 1.
(20) Walker, A. V.; Klötzer, B.; King, D. A. *J. Chem. Phys.* **1998**, *109* (16), 6879.
(21) Freyer, N.; Kiskinova, M.; Pirug, G.; Bonzel, H. P. *Surf. Sci.* **1986**, *166*, 206.
(22) Ducros, R.; Merril, R. P. *Surf. Sci.* **1976**, *55*, 227.
(23) Ducros, R.; Fusy, J. *Appl. Surf. Sci.* **1990**, *44*, 59.
(24) Wilf, M.; Dawson, P. T. *Surf. Sci.* **1977**, *65*, 399.
(25) Jackman, T. E.; Davies, J. A.; Jackson, D. P.; Unertl, W. N.; Norton, P. R. *Surf. Sci.* **1982**, *120*, 389.
(26) Comrie, C. M.; Weinberg, W. H.; Lambert, R. M. *Surf. Sci.* **1976**, *57*, 619.
(27) Wartnaby, C. E.; Stuck, A.; Yeo, Y. Y.; King, D. A. *J. Chem. Phys.* **1995**, *102* (4), 1855.
(28) McCabe, R. W.; Schmidt, L. D. *Surf. Sci.* **1976**, *60*, 85.
(29) Ertl, G.; Norton, P. R.; Rüstig, J. *Phys. Rev. Lett.* **1982**, *49*, 177.
(30) Gritsch, T.; Coulman, D.; Behm, R. J.; Ertl, G. *Appl. Phys. A* **1989**, *49*, 403.
(31) Gritsch, T.; Coulman, D.; Behm, R. J.; Ertl, G. *Phys. Rev. Lett.* **1989**, *63* (10), 1086.
(32) Imbihl, R.; Ladas, S.; Ertl, G. *Surf. Sci.* **1988**, *206*, L903.
(33) Eiswirth, M.; Krischer, K.; Ertl, G. *Appl. Phys. A* **1990**, *51*, 79.
(34) Krischer, K.; Eiswirth, M.; Ertl, G. *J. Chem. Phys.* **1992**, *96* (12), 9161.
(35) Bär, M.; Eiswirth, M.; Rotermund, H. H.; Ertl, G. *Phys. Rev. Lett.* **1992**, *69* (6), 945.
(36) Bär, M.; Falcke, M.; Zülicke, C.; Engel, H.; Eiswirth, M.; Ertl, G. *Surf. Sci.* **1992**, *269/270*, 471.
(37) Bär, M.; Gottschalk, N.; Eiswirth, M.; Ertl, G. *J. Chem. Phys.* **1994**, *100*, 1202.
(38) Bär, M.; Nettesheim, S.; Rotermund, H. H.; Eiswirth, M.; Ertl, G. *Phys. Rev. Lett.* **1995**, *74* (7), 1246.
(39) Bär, M.; Kevrekidis, I. G.; Rotermund, H. H.; Ertl, G. *Phys. Rev. E* **1995**, *52* (6), R5739.
(40) Bär, M.; Bangia, A. K.; Kevrekidis, I. G.; Haas, G.; Rotermund, H. H.; Ertl, G. *J. Phys. Chem.* **1996**, *100* (49), 19106.
(41) Levine, H.; Zou, X. *Phys. Rev. Lett.* **1992**, *69* (1), 204.
(42) Levine, H.; Zou, X. *Phys. Rev. E* **1993**, *48*, 50.
(43) Battogtokh, D.; Mikhailov, A. S. *Physica D* **1996**, *90*, 84.
(44) Battogtokh, D.; Preusser, A.; Mikhailov, A. S. *Physica D* **1997**, *106*, 327.
(45) Rose, K. C.; Battogtokh, D.; Mikhailov, A. S.; Imbihl, R.; Engel, W.; Bradshaw, A. M. *Phys. Rev. Lett.* **1996**, *76* (19), 3582.
(46) Falcke, M.; Engel, H. *J. Chem. Phys.* **1994**, *101*, 6255.
(47) Falcke, M.; Engel, H. *Phys. Rev. E* **1994**, *50*, 1353.
(48) Falcke, M.; Engel, H.; Neufeld, M. *Phys. Rev. E* **1995**, *52*, 763.
(49) Engel, W.; Kordesch, M. E.; Rotermund, H. H.; Kubala, S.; Oertzen, A. v. *Ultramicroscopy* **1991**, *36*, 148.
(50) Rotermund, H. H.; Jakubith, S.; Oertzen, A. v.; Ertl, G. *Phys. Rev. Lett.* **1991**, *66*, 3083.
(51) Eiswirth, M.; Ertl, G. *Phys. Rev. Lett.* **1988**, *60*, 1526.
(52) Krischer, K.; Eiswirth, M.; Ertl, G. *J. Chem. Phys.* **1992**, *97*, 307.
(53) Krischer, K.; Eiswirth, M.; Ertl, G. *Surf. Sci.* **1991**, *251/252*, 900.
(54) Woesler, R.; Schütz, P.; Bode, M.; Or-Guil, M.; Purwins, H.-G. *Physica D* **1996**, *91*, 376.
(55) Zhabotinsky, A. M.; Dolnik, M.; Epstein, I. R. *J. Chem. Phys.* **1995**, *103* (23), 10306.
(56) Or-Guil, M.; Bode, M.; Schenk, C. P.; Purwins, H.-G. *Phys. Rev. E* **1998**, *57*, 6432.
(57) Imbihl, R.; Sander, M.; Ertl, G. *Surf. Sci.* **1988**, *204*, L701.
(58) Rose, K. C.; Berton, B.; Imbihl, R.; Engel, W.; Bradshaw, A. M. *Phys. Rev. Lett.* **1997**, *79* (18), 3427.